Examining *slo* regulation of astrocyte morphology and neuronal excitability

By

Danielle Mathieson

A THESIS

Presented to the Neuroscience Graduate Program
at the Oregon Health and Science University
School of Medicine
In partial fulfillment of
the requirements for the degree of:

Master of Science in Neuroscience

October 2020

Contents

Acknowledgements

To start, I'd like to first acknowledge the people whose hard work directly allowed me to complete the experiments presented in this thesis. Yunsik Kang, PhD and Amanda Philippi performed the original astrocyte engulfment screen that first documented expression of $slo^{RNAi\text{-}104421}$ had effects on fly behavior. I would also like to thank Matt LaBella, PhD who sorted through Yunsik's original screen data and pulled out *slo* as a potentially interesting hit and started working with me on this project initially.

Next, I want to thank my mentor, Marc. The way he guided me through my graduate school experience has taught me so much about how to think like a scientist. I also deeply appreciate the unwavering support I received upon deciding to choose a career path outside of academia. Additionally, the support and direction from my committee members, Kelly, Kevin, and Mary, is greatly appreciated.

I would also like to thank all of the Freemanites, who were wonderful mentors and colleagues. They pushed me to be a better scientist and communicator and I'm thankful for all for the guidance I received from them.

Finally, I would like to thank my friends and family for all of the moral support.

Abstract

Astrocytes are a type of central nervous system glia that have critical roles within the brain, including supporting synapse formation, synaptic transmission, and maintaining proper circuit function. Using the fruit fly *Drosophila melanogaster* as a model system, we investigated the effects of knocking down *slowpoke* (*slo*) on astrocyte morphology and circuit function. *slo* is the *Drosophila* ortholog of the alpha subunit of a voltage and calcium gated potassium channel KCNMA1 in humans. Knockdown of *slo* just in astrocytes with RNAi produced varied results on astrocyte morphogenesis and animal behavior. Knockdown with $slo^{RNAi\text{-}104421}$ resulted in smaller astrocyte cell bodies in the L3 larval ventral nerve cord, despite normal astrocyte process infiltration into the neuropil. Expression of this RNAi line in astrocytes also led to motor defects in both larvae and adult male animals. Expression of additional RNAi lines in astrocytes did not recapitulate the astrocyte cell body phenotype or behavioral defects. Additionally, examination of astrocyte cell body size in *slo* mutants was also normal. In order to test whether expression of $slo^{RNAi\text{-}104421}$ was exerting its effects in a specific way to astrocytes, we expressed $slo^{RNAi\text{-}104421}$ in other glial subtypes within the larval VNC: ensheathing glia and cortex glia. Within these glial cell subtypes, general morphology of cells was normal, though cortex glia-expression of $slo^{RNAi\text{-}104421}$ produced loss of cortex glia cells in the thoracic region of the neuropil, supporting the hypothesis that $slo^{RNAi\text{-}104421}$ is targeting a gene with cell-specific roles. While the target of $slo^{RNAi\text{-}104421}$ could not be definitively attributed to *slowpoke*, it is clear that the gene it was disrupting had a profound impact on astrocyte morphology and animal behavior. This adds to the growing body of evidence that astrocytes modulate neuronal circuits and that disruption of astrocytes has profound effects on proper CNS function.

Chapter 1: Introduction

The nervous system's most basic form of communication occurs between neurons at synapses. However, only about half of the mammalian brain cells are neurons—the other 50% of the cells are glial cells. Originally thought to be "glue" that holds the neurons together, glial cells are now understood to be vital for the proper function of the nervous system. In the central nervous system, the brain and spinal cord, oligodendrocytes are a glial cell type that wrap axons with a specialized substance called myelin that insulates the axon and ensures proper electrical signal propagation[1]. Microglia are the brain's resident immune cells and also have emerging roles in nervous system development, specifically synaptic pruning[2]. Finally, astrocytes are a glial cell with highly branched processes that closely interact with synapses and blood vessels[3]. Decades of research has now demonstrated that astrocytes play roles in numerous facets of nervous system development and mature circuit functions, but are also implicated in many disease states[3].

In mammals, astrocytes originate from neural precursor cells called radial glia. These precursors will first give rise to neurons and then in the later stages of development, give rise to astrocytes and oligodendrocytes[4]. Astrocytes are named for their star-shaped morphology, but are characterized by their elaborate processes, which infiltrate the nervous system and come into contact with numerous structures. Astrocytes that are located in white matter are called fibrous astrocytes. Protoplasmic astrocytes are located in gray matter, have a bushier morphology, and are closely associated with synapses. Both types of astrocytes interact with blood vessels[5] and a single protoplasmic astrocyte can make contact with up to 100,000 synapses[6] in mice. Furthermore, astrocytes establish spatial domains, and upon an animal reaching adulthood, do not overlap their processes[6]. This tiling behavior of astrocytes, while not fully understood, is thought to be necessary for normal brain function because loss of tiling is associated with epileptic states[7].

Synaptic development

In adult animals, astrocytes are closely associated with neuronal synapses, physically surrounding them and forming what is now referred to as the tripartite synapse[8]. However, it was also speculated that astrocytes have an active role in synapse formation. This was first demonstrated using cultured retinal ganglion cells (RGCs) to show that astrocytes promoted excitatory synapse formation.

When retinal ganglion cells are cultured *in vitro*, they are capable of forming synapses, but they are relatively few, have low rates of spontaneous activity, and high failure rates in evoked transmission. However, culturing RGCs with astrocytes increased the number of synapses six- to seven-fold, as identified by immunostaining[9]. Furthermore, the frequency and amplitude of spontaneous activity is greatly increased with the addition of astrocytes to the RGC culture. The same result is found when media from cultured astrocytes is added to the RGCs, suggesting astrocytes release secreted factors sufficient to induce synapse formation[10].

Though the addition of astrocytes did increase the number of synapses formed as compared to glia-free cultures, the increase in synapse number was not enough to account for the much larger increases in spontaneous and evoked synaptic activity, suggesting the presence of astrocytes also enhances the efficacy of synaptic transmission[10]. We now know that astrocytes increase the efficacy of synapses through both pre- and post-synaptic mechanisms: increasing the number of vesicles released from pre-synaptic sites as well as inducing clustering of receptors on the post-synaptic side[9].

Further research has now identified several astrocyte-secreted factors that induce initial synapse formation and others that aid in refining or maturing synapses. These molecules include cholesterol complexed with apolipoprotein E (ApoE), thrombospondins (TSPs), hevin and the SPARC family of proteins, and TGFβ, though their mechanisms and effectiveness depend on both brain region and developmental time point being examined[11].

Cholesterol bound to ApoE was the first astrocyte-secreted compound identified that increased both synapse number and the efficiency of synaptic transmission in cultured RGCs[12]. Cholesterol is highly concentrated within the synapse, so it is likely cholesterol availability that contributes to proper synapse generation. Neurons produce little cholesterol themselves and therefore rely on astrocytes to provide exogenous cholesterol to generate both dendrites and synapses[13]. More recent research has indicated that cholesterol is required for synapse maturation and that perturbing astrocyte cholesterol synthesis leads to an increased number of immature dendritic spines[14].

Further research identified additional astrocyte-secreted molecules that promote synapse formation. Thrombospondins are oligomeric extracellular matrix proteins required for synaptogenesis both *in vitro* and *in vivo*. One receptor for TSPs identified was the α2δ-1 voltage-gated calcium channel subunit[15], but TSPs can additionally signal through neuroligins and integrins[16, 17]. Hevin, a matricellular protein in the SPARC family, is also synaptogenic, but is antagonized by a related protein, SPARC—both of which are secreted by astrocytes. Hevin promotes synapse formation by acting as a "bridge" between presynaptic neurexin-1alpha and post-synaptic neuroligin-1B—two isoforms that normally do not interact[18]. SPARC also plays an additional role of inhibiting synaptogenesis by prohibiting integrin-mediated accumulation of AMPA receptors[19]. Due to the lack of evidence for SPARC directing binding and inhibiting hevin, it is likely that it functions through a dominant-negative mechanism by binding to hevin's targets and preventing hevin signaling. That astrocytes can secrete both a synaptogenic molecule and its inhibitor, places them in a unique position to fine tune the formation of synapses in a given brain region.

Interestingly, TSPs and hevin were sufficient to induce the formation of structural, albeit not functional, excitatory synapses in RGCs[20, 21]. The induced synapses contained NMDA receptors, but lacked AMPA receptors, rendering them "silent synapses". This demonstrates that astrocytes release

additional factors that participate in the maturation of a structural synapse to an electrically functional one.

One such family of molecules involved in this synapse maturation are the glypicans, specifically Gpc4 and Gpc6, which not only increase the number of synapses when added to RGC cultures, but render them functionally active by clustering GluA1 receptors on the post-synaptic membrane[22]. Glypicans are hypothesized to function by binding to LAR (Leukocyte common antigen–related proteins), which have also been shown to be synaptogenic in *Drosophila* and cultured rat hippocampal neurons[22-24].

Though a number of synaptogenic molecules have been identified, their effects may depend on neuronal subtype and region-specific signaling. While astrocytes or astrocyte-conditioned media have been shown to promote synaptogenesis in cultured RGCs, hippocampal neurons, cortical neurons, and Purkinje cells, the exact molecules required by each neuronal subtype differs. For example, TGF-β stimulates the release of D-serine which can induce functional excitatory synapses in cortical neurons, but has no effect on synaptogenesis in RGCs[25]. Similarly, TSPs are highly synaptogenic to RGCs, but have no effect on the final number of synapses in hippocampal neurons, though they do increase the initial rate of synapse formation[16]. It is therefore likely that discrete signaling molecules are utilized at specific developmental time points, and in different proportions, to generate synapses in distinct neuronal subtypes.

All of the previously described synaptogenic molecules were required for the formation of excitatory synapses. However, astrocytes also instruct the formation of inhibitory synapses, though to date, none of the molecules implicated in excitatory synapse formation are required for this process and inhibitory-specific cues have proven to be elusive[26]. Because astrocytes contribute to the development of both excitatory and inhibitory synapses, they are placed in a potentially important position to instruct

excitatory/inhibitory (E/I) balance within the nervous system: something that goes awry in several neurodevelopmental disorders, including Autism Spectrum Disorder (ASD) and schizophrenia[17].

Synaptic Pruning

What may seem paradoxical is that during development, the nervous system overproduces synapses, which are then pruned back to optimize circuit functions. A majority of synaptic pruning is performed by microglia, the brain's resident immune cells, but astrocytes also contribute to synaptic pruning during development. Sometimes the same molecular players that are used to build synapses initially are reutilized to eliminate synapses after circuits have been built. Failure to refine synaptic connections is associated with developmental disorders such as ASD, schizophrenia, and epilepsy[27]. Additionally, synaptic loss is an early hallmark of neurodegenerative disorders, raising the question of whether glial dysfunction directly leads to disease.

The visual system has not only been a well-utilized model to study synapse formation, but also one to study synapse refinement. RGCs project their axons from the retina, through the optic nerve, to the dorsal lateral geniculate nucleus (dLGN) in the thalamus, where they make synaptic connections. Initially, target neurons within the dLGN will have synaptic inputs from 10-12 RGCs from both eyes. Then, the majority of synaptic contacts from the ipsilateral eye will be pruned away, leaving a majority of contralateral inputs. These contralateral synapses will then be further refined until 1-4 synapses onto each neuron remains. Neuronal activity has been demonstrated to be crucial to this refinement because blocking spontaneous neural activity in the retina prevents synapse refinement[28].

In this system, astrocytes, with some contribution from microglia, engulf synapses during this period of synaptic refinement. The engulfment receptors MEGF10 and MERTK are required for astrocytes to engulf synapses[29], thus indicating they utilize a distinct mechanism from microglia, which primarily utilize the complement cascade to identify synapses to be removed[30]. Furthermore, this demonstrates the conserved ability of astrocytes, and glial cells in general, to engulf synapses. Draper

and Ced-1, the *Drosophila* and *C. elegans* orthologs of MEGF10 are also required for neuronal remodeling during development[31-33].

Using another sensory relay pathway to examine pruning has uncovered an additional mechanism for how astrocytes participate in synaptic pruning. Neurons from the principal trigeminal nucleus (Pr5) in the hindbrain project to the ventral posterior-medial thalamic nucleus (VPm), which relays information to the somatosensory cortex. Initially, VPm neurons receive numerous synaptic inputs from Pr5 neurons, but these are pruned to a single input. Astrocytes release ATP in response to activation of inositol 1,4,5-trisphosphate type 2 receptors (Itpr2), an astrocyte-specific Ip3 receptor that releases calcium from intracellular stores. The ATP then binds to P2Y receptors, likely located on neurons, to mediate synaptic pruning[34].

The role of astrocytes in synaptic refinement and neuronal remodeling is contested as to whether astrocytes play an instructive part in determining which synapses are engulfed. In the visual system, the weakest inputs from RGCs are eliminated during synaptic refinement and spontaneous neuronal activity is required for astrocytes to engage in synaptic pruning, suggesting a cell-autonomous role for neurons determining which synapses are eliminated and glial cells executing phagocytosis. However, astrocyte-secreted TGFβ is required to increase neuronal expression and synaptic localization of C1q, the initiating factor in the complement cascade that binds CR3 on microglia to induce engulfment[30, 35]. This supports a model in which multi-directional signaling between astrocytes, neurons, and microglia is required for proper synaptic refinement in the visual system. Furthermore, astrocytes release the cytokine IL-33, which signals to microglia and is required to establish the proper number of synapses in the spinal cord and thalamus[36].

Astrocytes also play a role in synaptic refinement that is more complex than simply reducing the number of synapses—they also help shape exactly what type of inputs a neuron receives. In the visual cortex, individual dendritic spines can receive multiple excitatory synaptic inputs, adding complexity to

the dogma that each dendritic spine receives a single synaptic input. In the visual system, both thalamic and intra-cortical inputs are received and can initially be present on a single dendritic spine. However, through a process of refinement, each dendritic spine is left with a single input that is either of cortical or thalamic origin. Loss of Hevin, an astrocyte-secreted synaptogenic molecule described above, prevents the proper refinement of multiple inputs onto dendritic spines and the number of spines with multiple excitatory inputs persists into adulthood in Hevin-knockout mice. Furthermore, while the total number of excitatory synapses in this region is normal in hevin-knockout mice, the number of specifically thalamic inputs is reduced[37]. This indicates astrocytes play a role in shaping the type, as well as the number, of synapses in a given region.

NT re-uptake/ transporter expression

A critical function of astrocytes at the synapse is to clear neurotransmitters to modulate synaptic transmission. Astrocytes express a number of neurotransmitter transporters, including excitatory amino acid transporters (EAATs)[38], GABA transporters (GATs)[39], and glycine transporters (GlyTs)[40].

Of the five members in the EAAT family, EAAT1 (GLAST) and EAAT2 (GLT-1) are largely produced by astrocytes, whereas EAAT3 - 5 are produced specifically by neurons. Loss of EAAT2, either globally or specifically in astrocytes, results in increased extracellular glutamate and neuronal hyperexcitability that results in seizures and death, but loss in neurons has no behavioral effect[41, 42]. Loss of EAAT1 results in motor discoordination, and while it does not confer seizure susceptibility, experimentally induced seizures are longer than normal[43, 44]. Whole-animal knockout of neuronal-specific EAATs does not result in seizure behavior or death[45], emphasizing the importance of astrocytic clearance of glutamate in regulating excitatory balance for normal brain function.

At synapses within both the cerebellum and hippocampus, pharmacological blockade of glutamate transport prolongs the duration of excitatory post synaptic currents (EPSCs)[46-48]. However,

the importance of rapid glutamate clearance from the synapse by astrocytes seems to depend on brain region and neuronal subtype because of the differences in astrocytic coverage of synapses between regions. Within the cerebellum, astrocyte coverage is almost 100%, but is estimated to be only 60% within the hippocampus[49]. Therefore, while on a global scale, astrocyte uptake of glutamate is important to brain health and survival, the requirement at individual synapses may vary.

Gliotransmission

Once the circuits and synaptic connections within the brain are developed, changes in synaptic strength can still occur and are thought to underlie the basis for learning and memory. Long-term potentiation (LTP) and long-term depression (LTD) are two classically studied mechanisms to alter synaptic strength and astrocytes may play a role in both of these processes. One way for astrocytes to do this is by releasing "gliotransmitters", molecules released into the synapse that will alter synaptic responses, but the evidence of astrocytes utilizing this mechanism *in vivo* is limited.

In slice preparations, astrocytes have been shown to release D-serine, a co-agonist for NMDA receptors, thus facilitating LTP[50, 51]. Additionally, in a SNARE-dependent mechanism, astrocytes release ATP, which is converted to adenosine extracellularly. This adenosine binds A1 receptors on neurons, decreasing basal synaptic transmission, but increasing the dynamic range available for LTP induction[52]. Other gliotransmitters include glutamate and tumor necrosis factor α (TNRα).

Gliotransmission is thought to be regulated by astrocytic calcium elevations, and various studies that chelate astrocytic intracellular calcium have been shown to effect synaptic transmission [53]. Astrocyte calcium elevations have been directly placed in a neuromodulatory pathway that mediates circuit function and behavioral output in *Drosophila*[54]. Tdc2 neurons receive signals from upstream olfactory neurons, release tyramine and octopamine, the flu homologs of norepinephrine, which binds the octopamine/tyramine receptor (Oct-TyrR) on astrocytes. This increases calcium within the astrocytes via the TRP channel Water witch, leading to release of ATP that binds the purinergic receptor AdoR on

downstream dopamine neurons. This signaling inhibits the activity of the dopamine neurons and allows for normal chemosensory and mechanosensory behaviors to occur[54]. The components of this pathway are also highly conserved, which suggests similar neuromodulatory pathways that include astrocytes are present in vertebrate organisms.

Ion buffering

The buffering of potassium is critically important for circuit function because excessive increases in extracellular potassium leads to hyperexcitability in neurons. One important role for astrocytes is buffering the potassium that accumulates extracellularly during neuronal firing.

Astrocytes can regulate potassium uptake through multiple mechanisms broadly categorized into 'net uptake' or 'spatial buffering'. The first refers to active transport of ions across the membrane and is dependent on the sodium potassium exchanger Na^+/K^+-ATPase (NKA). This enzyme hydrolyzes ATP to exchange three sodium ions out of the cell for two potassium ions into the cell—against their electrochemical gradients. This exchanger actively sets the membrane potential and maintains basal levels of extracellular potassium[55]. Upon increases of neuronal activity that increases extracellular potassium more than a modest amount, additional mechanisms promote extracellular potassium clearance, such as the $Na^+/K^+/2Cl^-$ cotransporter (NKCC), which transports sodium, potassium, and chloride across the membrane concurrently with water, resulting in increases in astrocyte volume[56].

Spatial buffering refers to mechanisms by which potassium is diffused away from areas of high to low concentration within astrocytes. This mechanism was first proposed by Orland et al in 1966 and later demonstrated in individual Müller glia—a specialized glial subtype in the retina. Müller glia "siphon" potassium from their distal ends and deposit it into vitreous fluid via their endfeet[57, 58] and can also increase potassium extracellularly in the retina if it becomes abnormally low[59].

The spatial buffering mechanism in other brain regions relies in part on the combination of astrocyte gap junctions and their expression of inward-rectifying potassium channels (Kir channels).

Inward-rectifying channels are so named because they more easily pass current inward due to high-affinity pore blocks at the more positive potentials that would normally promote ion efflux. Astrocytes normally have a negative resting potential, but it is usually still higher than the reversal potential for potassium, which would promote potassium efflux from the cell. However, as extracellular potassium increases, the reversal potential for potassium becomes more depolarized, allowing a switch from efflux to influx. One problem with this mechanism is that potassium influx into an astrocyte should depolarize the membrane and reduce the potassium driving force into the cell. One hypothesis is that astrocytes combat this is by quickly diffusing intracellular potassium away from high-concentration regions to low concentration regions via astrocyte gap junctions. Indeed, it has been found that gap junction coupling stabilizes the astrocyte membrane potential by conferring isopotentiality to coupled astrocytes[60]. This mechanism is thought to stabilize the astrocyte membrane potential to allow for more efficient potassium clearance. Additional data show that astrocytes in slice preparations that are deficient in connexins 30/45 (Cx30/Cx45) are associated with increased potassium accumulation at synapses within the stratum lacunosum moleculare, but not the stratum radiatum—both regions within CA1 in the hippocampus[61]. Furthermore, It was found that Cx30/Cx45 mediated currents only accounted for 30% of the currents within an astrocyte[61], so additional buffering mechanisms occur that may be region-specific.

The role of Kir channels in spatial buffering has been largely studied by using Kir-specific pharmacological blockers, such as barium. In slice preparations from the guinea pig olfactory cortex, addition of barium stopped a stimulation-induced increase of potassium within the astrocytes[62], but did not abolish it, suggesting Kir channels and ion transporters both contribute to potassium uptake.

Deficiencies in the ability of astrocytes to buffer potassium is associated with disease states such as epilepsy. If extracellular potassium concentrations get too high, hyperexcitability within neurons results. In support of this hypothesis, a significant barium-sensitive inward potassium current was found

in control patient hippocampal slices following stimulation, but this uptake was impaired in astrocytes taken from patients that had therapy-refractory temporal lobe epilepsy[63].

While a number of Kir channels may contribute to potassium buffering, the one of particular interest is Kir4.1 due to its high expression in astrocytes over neurons. RNAi-mediated knockdown of Kir4.1[64] or conditional knockout in astrocytes impaired potassium uptake[65, 66]. Additionally, the conditional knockout presented behaviorally with ataxia, stress-induced seizures, and died prematurely[65]. Furthermore, mutations in Kir4.1 is associated with seizure disorders in human patients[67].

However, other studies have not seen a requirement for Kir4.1 in potassium clearance[68, 69] and invoke the action of the NKA. Since many experiments have shown partial contributions for gap junctions and Kir4.1 channels, it is likely a combination of all mechanisms, including additional Kir channels, that contribute to potassium clearance and regulation. Regional differences in neuronal subtypes, activity levels, cellular architecture, and much more may determine the relative contributions for both net uptake and spatial buffering to maintain potassium homeostasis.

BK potassium channels

Ion channels within the nervous system are required to establish a resting membrane potential, generate action potentials within neurons, and allow cell-to-cell signaling to occur. Astrocytes express a number of different ion channels, including a variety of potassium channels, which are the ion channel type primarily responsible for establishing the astrocyte resting membrane potential. However, a number of other potassium channels also serve a variety of other functions within the cell.

One class of potassium channels are BK channels, also called MaxiK channels, named for their large conductance. BK channels are expressed by both neurons and astrocytes and can be activated by both increases in membrane potential and by increases in intracellular calcium. In neurons, the major functions of this channel appear to be regulating the shape of action potentials and changing firing rates

and neurotransmitter release by lowering membrane potential in response to the coincidence detection of voltage increases and rise in intracellular calcium[70].

In mammalian astrocytes, BK channels are primarily localized to astrocytic endfeet, as demonstrated by double-immunolabeling of GFAP and the rat BK channel or dye filled astrocytes combined with antibody-labeled BK channels. In both the cerebellum and hippocampus, strong co-localization occurred between astrocytic perivascular endfeet and BK channels, which was further confirmed by electron microscopy[71]. Punctate staining of BK channels was also detected within the astrocyte soma and larger processes, but to a much lesser extent compared to the endfeet. The distribution of BK channels is also similar to that of AQP4, an astrocyte-expressed water channel[71]. Therefore, BK channels are present in the astrocytic endfeet, where regulation of blood flow occurs.

Studies show that the diameter of vasculature in the brain is sensitive to levels of extracellular potassium[72, 73]). This observation, combined with the presence of BK channels at astrocytic endfeet, and the morphological presence of astrocytic endfeet around blood vessels, it was hypothesized that astrocyte-expressed BK channels might be involved in neurovascular coupling. To demonstrate the requirement for BK channels, a combination of pharmacology and electrophysiology was used in cortical slice preparations. In slices, neuronal stimulation leads to BK channel currents on the endfoot[74]. The opening of BK channels releases potassium into the perivascular space which activates Kir channels on smooth muscle cells, leading to changes in arterial diameter[74]. Intriguingly, the same mechanism is used to induce dilation or constriction and depends on the levels of calcium within the endfoot and the subsequent potassium concentration in the perivascular space. Modest levels of astrocyte calcium result in modest increases in potassium to induce vasodilation, whereas large calcium and subsequent potassium increases result in vasoconstriction[75].

In addition to regulating neurovascular-coupling, in models of vascular amyloid deposition, BK channels, along with hallmark astrocyte genes such as GFAP, AQP4, and Kir4.1 are downregulated, potentially linking disruption of BK channel function with AD pathogenesis[76].

Drosophila melanogaster as a model organism to study astrocyte development and function

Flies are an ideal model organism to probe the mechanisms of gene function within specific cell types for multiple reasons. The fly nervous system, while simple compared to mammalian brains, has hundreds of thousands of neurons and glia that control complex behaviors. Additionally, the genome of the fly is highly homologous to the human genome which allows for the translatable analysis of gene function. The fly as a model system also has a wealth of genetic tools to manipulate and visualize specific cell types, which can even be done at the single-cell level.

Fly astrocytes are functionally and morphologically similar to mammalian astrocytes. They robustly express neurotransmitter transporters, such as EEATs and GAT, which uptake glutamate and GABA, respectively. Morphologically, fly astrocytes also have bushy, dense processes that invade the synaptic neuropil and closely associate with synapses[77]. Additionally, fly astrocytes recapitulate another feature of mammalian astrocytes, which is regulation of vasculature and gas exchange. In mammals, astrocytes regulate blood flow through signaling with endothelial cells via their endfeet[74, 75]. In flies, gas exchange occurs through the cells that make up the trachea, which extends branches and processes into tissues. Local reactive oxygen species (ROS) production activates TrpML channels on astrocytes, which generates microdomain calcium transients. These calcium transients negatively regulate trachea filopodia extension, presumably to avoid hyperoxic conditions[78]. Due to these similarities, and because of the tools available in flies, manipulating fly astrocytes and studying the effects on structure and function could give insights into widespread astrocyte functions with a speed and on a scale not possible in mammalian model systems.

One such genetic tool available in the fly is the GAL4/UAS system[79], which allows for cell-specific expression and manipulation. GAL4 is a yeast transcription factor that binds to UAS sequences, which are not found in the *Drosophila* genome. Transgenic flies that express GAL4 under a cell-specific promoter are crossed to UAS transgenic flies that can have a variety of constructs following the UAS sequence in order to achieve cell-specific expression. The constructs that follow the UAS sequence can be markers such as GFP, cDNAs to induce overexpression of certain genes, or even short sequences that will inhibit gene expression before translation, known as RNA interference (RNAi). The use of RNAi for probing gene function has some benefits over using whole-animal mutants, the first of which is cell-type specificity. Additionally, knockdown of genes with RNAi may result in phenotypes in which a whole-animal null mutation would be lethal. Finally, screening with RNAi is an efficient process: a single stock of the GAL4 driver line can be maintained to cross to any number of different UAS-RNAi lines, which are easily ordered from stock centers.

In our lab, disrupting individual genes with RNAi specifically in astrocytes has identified genes required for astrocyte morphogenesis and function. Knocking down the FGF receptor *Heartless* inhibits normal astrocyte growth and morphogenesis[77]. Additionally, astrocyte-specific RNAi-mediated knockdown of the genes encoding Tensin, β-integrin, and other focal adhesion molecules enhanced recovery from seizures conferred by either a genetic mutation in adults or picrotoxin-induced motor deficiencies in larvae.

In the data presented in this thesis, I utilized the tools described above to express an RNAi line targeting the BK channel gene *slowpoke* and characterize its effects when expressed specifically in astrocytes. The work described adds to the growing body of knowledge that perturbing astrocytes has profound effects on both circuit and animal behavior.

Chapter 2: Results

Introduction

As *Drosophila* develop, they undergo a metamorphosis where they transform from larvae to adults. During metamorphosis, the entire nervous system is rewired: neurites are pruned back and then re-grow and many neurons undergo programmed cell death. The cellular debris that is created from this neuronal remodeling is engulfed by surrounding glial cells. Early into metamorphosis, *Drosophila* astrocytes transform into phagocytic cells that engulf neuronal debris. A screen was performed in the lab for genes expressed in astrocytes required for this engulfment process. A collection of RNAi lines targeting signaling molecules (secreted molecules and proteins containing transmembrane domains) were included in the collection, totaling about 1500 fly lines. Each of these RNAi lines was crossed to a GAL4 driver line that expressed membrane-tethered GFP and GAL4 only in astrocytes. Brains were then dissected from larval and pupal stages, fixed, mounted, and imaged to determine if the gene each RNAi line targets is required for engulfment that occurs within the first 12 hours of metamorphosis. The presence of neural debris at 12 hours indicated a positive hit. The progeny of each cross were also allowed to develop past metamorphosis into adulthood to determine whether knocking down each gene was lethal at any developmental time point. This screen led to a number of different classes of hits. The first class were genes that prevented engulfment, but had morphologically normal astrocytes, indicating that the gene likely had an engulfment-specific role. The second class were hits that prevented engulfment, but had astrocytes with abnormal morphology, suggesting that general loss of astrocyte health or function prevented engulfment. A third type of hit were genes that when knocked down only in astrocytes, caused lethality at any time point examined. A subset of this class included hits that appeared to cause lethality in early post-eclosion adults, but had no effect on astrocyte morphology

early in development. This served as my entrance to the project to further examine these lethal genes and their effects on astrocyte morphology and function.

One RNAi line that was of particular interest to me was *slo*$^{RNAi\text{-}104421}$, which targets slowpoke (*slo*), the alpha subunit of a BK Potassium channel. This RNAi line was originally thought to have morphologically normal astrocytes in larvae, but cause lethality in early post-eclosion adults. Upon re-crossing this line to the strong astrocyte-specific driver, *GMR25H07-GAL4* (subsequently referred to as *alrm-max-GAL4*) I discovered that knocking down *slo* in astrocytes was not in fact lethal, but adults were highly uncoordinated. I collected freshly eclosed adults and flipped them onto new food vials every few days. They could not climb the side of the vial without falling and had shaking movements. This highly uncoordinated behavior likely led to adults becoming stuck in the fly food at the bottom of the original vial and dying, thus the initial characterization of lethality.

Another screen performed in the lab, with largely overlapping RNAi lines to the astrocyte-engulfment screen, was looking for genes involved in development of wrapping glia, a glial subtype in the peripheral nervous system that wraps peripheral axons, morphologically similar to Remak Schwann cells in mammals. The same RNAi line identified in the astrocyte-engulfment screen, *slo*$^{RNAi\text{-}104421}$, was found to prevent proper development of wrapping glia (unpublished data). This could indicate a more general role for *slo* in glial development.

Finally, a third screen performed in the lab screened for enhancers and suppressors of a phenotype caused by a mutation in the gene *easily-shocked (eas)*, a choline/ethanolamine kinase. Knockout of *eas* results in seizure activity after mechanical disturbance. Vortexing *eas* mutant flies in empty vials results in seizure behavior, but flies recover within a few minutes. This screen knocked down genes only in astrocytes in an *eas* mutant background to test whether loss of specific genes only in astrocytes suppressed or enhanced the seizure phenotype. When *slo*$^{RNAi\text{-}104421}$ was expressed only in astrocytes, the seizure phenotype was greatly enhanced beyond that of *eas* mutant alone[80], with only

79% of the flies recovering by 4 minutes, which was the final time point for the screening assay (unpublished data).

Overall, this preliminary data from multiple screens implicated *slo*$^{RNAi\text{-}104421}$ as targeting an important gene required for functions of multiple glial subtypes. The gene it disrupts seems to play a role in development of the complex morphology that wrapping glia exhibit in the peripheral nervous system by wrapping axons. Additionally, it had a profound impact on fly motor behavior when knocked down in astrocytes alone or concomitantly with whole-animal loss of *eas*, which drastically worsened seizure behavior. BK potassium channels have important functions in neurons for shaping action potentials and acting as negative feedback regulators to calcium increases. Additionally, the mammalian homolog of *slo* is required in astrocytes to regulate blood flow. The possibility that this gene could be important for glial development and perhaps more specifically, astrocyte function and E/I balance within the nervous system led me to further investigate this gene.

Results

Examination of astrocytes in L3 brains had normal astrocyte process infiltration into the neuropil, but abnormally small cell bodies after expressing *slo*$^{RNAi\text{-}104421}$

I decided to more closely examine astrocyte morphology in larval brains with astrocyte-specific expression of *slo*$^{RNAi\text{-}104421}$. I crossed the *alrm-max-GAL4, UAS-mcd8-GFP* to the *UAS-slo*$^{RNAi\text{-}104421}$ line and examined astrocyte morphology in VNCs of wandering third-instar larvae. The infiltration of astrocyte processes into the neuropil was grossly normal in *slo*$^{RNAi\text{-}104421}$ flies compared to controls (Fig 1). However, cell bodies of astrocytes were significantly smaller in the *slo*$^{RNAi\text{-}104421}$ animals compared to controls (Fig 1).

To determine if this was a cell-autonomous effect, I utilized a “flp-out” strategy that labels astrocytes with membrane-tethered GFP under the control of an *alrm-LexA* driver. Expression of a flippase sporadically “flips out” the LexA construct early in astrocyte development and allows for

expression of GAL4 to drive expression of UAS-mCherry. Thus a subset of astrocytes will be labeled with mCherry in a small number of clusters of clones. Crossing this line to UAS-RNAi lines also allows knockdown of the target gene in just the mCherry labeled cells, allowing for clonal manipulation and visualization. I found that in flp-out astrocyte clones that expressed *slo*$^{RNAi\text{-}104421}$, the small cell body phenotype still occurred, despite the majority of the surrounding astrocytes appearing normal in size, arguing for a cell-autonomous effect of *slo*$^{RNAi\text{-}104421}$ expression on cell body size (Fig 1). Consistent with our whole-animal observations, even in flp-out clones, astrocyte infiltration appeared grossly normal with no gaps (Fig 1).

What effect does expressing *slo*$^{RNAi\text{-}104421}$ have on other glia subtypes?

slo$^{RNAi\text{-}104421}$ emerged as a hit in screens that were specifically targeting astrocytes and wrapping glia. In one screen, *slo*$^{RNAi\text{-}104421}$ emerged as an enhancer of the *eas* mutant, which is a bang-sensitive mutation that causes seizure behavior from mechanical disturbance. I was able to confirm that *eas* mutant flies also expressing *slo*$^{RNAi\text{-}104421}$ in astrocytes recovered slower than control alone (Fig S1). I then wanted to investigate the effect on cell morphology when expressing *slo*$^{RNAi\text{-}104421}$ in other glia subtypes. Ensheathing glia are a *Drosophila* glial subtype that surround the edges of the neuropil and are critically important for engulfment of neuronal debris after injury[81]. Cortex glia surround and enwrap neuronal cell bodies, which are found outside the neuropil region [82]. I crossed *slo*$^{RNAi\text{-}104421}$ to either *GMR54H02-GAL4 or GMR83E12-GAL4*, driver lines that express in cortex glia and ensheathing glia, respectively. Expression of *slo*$^{RNAi\text{-}104421}$ appeared to have no effect on the morphology of either glia cell type (Fig 2). However, expression of *slo*$^{RNAi\text{-}104421}$ in cortex glia resulted in loss of cells specifically in the thoracic region of the VNC, as demonstrated by a maximum intensity projection (Fig 2), which is of note because specialized neural stem cells lie in this area and they are supported by cortex glia in complex ways [83]. This result may indicate that the cell-cell signaling in this region may differ from other regions of the VNC or greater CNS, leading to increased susceptibility of these cells to perturbation.

Confirming the target of *slo*$^{RNAi\text{-}104421}$

In order to try to confirm that the RNAi line that was producing phenotypes was targeting the intended gene, *slowpoke*, we ordered additional independent RNAi lines. Two of the RNAi lines targeted non-overlapping regions of *slo* compared to *slo*$^{RNAi\text{-}104421}$, but the third, *slo*$^{RNAi\text{-}6723}$, overlapped about half of its target sequence with *slo*$^{RNAi\text{-}104421}$. The first line tested, *slo*$^{RNAi\text{-}55405}$ failed to recapitulate morphological and behavioral phenotypes that *slo*$^{RNAi\text{-}104421}$ line produced (Figs 3,5). Two additional lines, *slo*$^{RNAi\text{-}6723}$ and *slo*$^{RNAi\text{-}26247}$ also failed to recapitulate the astrocyte morphological phenotype (Fig 3). Behavioral phenotypes were not tested in these lines.

Next, I performed GAT staining on L3 larval brains of presumed *slo* mutant larvae: *slo*^{1} and *slo*^{11481}. GAT, the only *Drosophila* GABA transporter, is highly expressed by astrocytes in the larval VNC and is present on the plasma membrane[77]. This allows for GAT staining to be used as a marker to examine cell morphology. I dissected L3 larvae and stained with GAT to determine whether *slo* mutant larvae have the same cell body phenotype as *slo*$^{RNAi\text{-}104421}$. The *slo*^{1} mutant had a similar average astrocyte cell body size compared to control (Fig 4). The *slo*^{11481} mutant had statistically smaller cell bodies compared to control, but the difference in absolute values was much smaller than the size difference that expression of *slo*$^{RNAi\text{-}104421}$ produced (Fig 4, Fig 1). Whole-animal *slo* mutants have motor defects, but these are proposed to be caused by dysfunction in neurons because *slo* is widely expressed throughout the nervous system.

I attempted to demonstrate that the *slo* mutant lines were null alleles of *slo* using reverse-transcription PCR. However, I detected the *slo* transcript in whole animal RNAi isolated from both *slo*^{1} and *slo*^{11481} (Fig S2). Detection of transcript from the *slo*^{1} mutant was not unsurprising because this mutation has not been characterized in detail and may be a hypomorphic mutation. However, it has been previously reported that the *slo*^{11481} mutant has loss of transcript[84]. Further analysis would be required to definitively determine the nature of these alleles.

Are there behavioral consequences of astrocyte-specific expression of *slo*$^{RNAi\text{-}104421}$?

Though other fly lines could not confirm the specificity of *slo*$^{RNAi\text{-}104421}$ to *slo,* early observations demonstrated that flies expressing this line were uncoordinated were investigated further. *Drosophila* have an innate escape behavior, called negative geotaxis, in which they will move opposite gravity when agitated[85]. This innate behavior is often used to measure locomotion abilities: healthy flies will quickly crawl up the side of a vial when tapped down to the bottom and remain at the top of the vial for several minutes. Defects in locomotion can be quantified by measuring how many flies are unable to reach a certain height within the vial in a given time period. Astrocyte-specific expression of *slo*$^{RNAi\text{-}104421}$ caused uncoordinated phenotypes in adult animals early after eclosion as quantified using this negative geotaxis assay. Male adults expressing *slo*$^{RNAi\text{-}104421}$ in astrocytes had a severe defect, with only 20% of the flies passing the cut-off line compared to around 75% of control flies (Fig 5). However, female adults expressing the RNAi performed as well as control flies of either sex (Fig 5). I then decided to test whether motor defects manifested earlier in development to determine at which developmental time point the RNAi expression might be disrupting astrocyte function. Using a larval motor tracking assay, I measured how far larvae could crawl in a one-minute time span. Expression of *slo*$^{RNAi\text{-}104421}$ in astrocytes caused a small, but significant decrease in larval crawling distance compared to controls (Fig 5). Animals in this experiment were not separated by sex. This indicates that *slo*$^{RNAi\text{-}104421}$ expression affects motor output early in the development of the animal and persists into adulthood.

Chapter 3: Discussion

The role of potassium channels in the nervous system has been extensively studied. In neurons, voltage-gated potassium channels function to repolarize the membrane after an action potential. Inward-rectifying potassium channels aid in stabilizing the membrane potential after GPCR signaling, such as activation of GIRKs from G proteins. In astrocytes, inward-rectifying potassium channels also play a major role in potassium buffering—a key role within the nervous system. BK channels in neurons repolarize the membrane after action potentials and regulate neurotransmitter release at the synaptic terminal. BK channels have also been implicated in astrocytic endfeet to regulate blood flow. Though BK channels have been shown to be critical in optimal nervous system function in both neurons and glia in an adult brain, little research has been done in the role of potassium channels in astrocyte development and morphogenesis. The possibility that a BK channel might be involved in astrocyte morphogenesis and function led me to further characterize the *slo*$^{RNAi\text{-}104421}$ line and try to confirm this line's specificity to *slo*, the *Drosophila* homologue of the *KCNMA1* (BK channel pore-forming subunit) gene.

The *slo*$^{RNAi\text{-}104421}$ line was identified as a modulator of astrocyte function because it was thought to cause lethality in recently-eclosed adults when expressed only in astrocytes. Further examination of astrocyte-expression of this line determined that only male adults were severely uncoordinated, as was quantified with a negative geotaxis assay, and females were unaffected. These motor defects arise earlier in the life of the animal as larval crawling behavior was impaired, though sex-specific analysis was not performed. Whole-animal *slo* mutants also have motor defects, but because *slo* is widely expressed throughout the nervous system, it has been previously hypothesized that neuronal loss of *slo* causes these behavioral phenotypes. One way this could be tested is examining whether astrocyte-specific expression of a *slo* transgene in an otherwise null animal rescues behavior. This would indicate that astrocyte-specific loss of *slo* causes the behavioral defects.

Astrocyte-expression of this RNAi line also led to abnormal cell body morphology, despite normal infiltration of astrocyte processes into the neuropil. However, three additional RNAi lines also targeted to *slo*, $slo^{RNAi\text{-}55405}$, $slo^{RNAi\text{-}26247}$, and $slo^{RNAi\text{-}6723}$, did not recapitulate the abnormal cell body phenotype observed in the original $slo^{RNAi\text{-}104421}$ line. One of the lines, $slo^{RNAi\text{-}55405}$, also did not recapitulate the larval crawling defect. Though additional RNAi lines failed to recapitulate the $slo^{RNAi\text{-}104421}$ phenotype, it is possible that these RNAi lines are inefficient in knocking down *slo*.

I examined the morphology of astrocytes in fly lines that were presumed *slo* mutant lines to test this possibility. Both mutant lines had astrocyte cell bodies that were morphologically similar to control astrocytes and did not recapitulate the phenotypes seen from expression of $slo^{RNAi\text{-}104421}$. This would suggest that *slo* is not required for astrocyte development. However, I was unable to confirm that either mutant line contained a null allele for *slo*. The slo^{1} mutant was generated from EMS mutagenesis. Potassium currents measured from this line are severely reduced, suggesting this mutation is either a null or at least an extreme hypomorph, but the exact mutation in this line is not known. The second mutant line, slo^{11481}, is a MiMIC line with an insertion into the second exon of *slo* that should result in an early stop codon and prohibit production of full-length transcripts. However, using reverse-transcription PCR, I was unable to confirm the loss of *slo* transcripts, despite being reported for the slo^{11481} line previously[84]. Detection of transcript from slo^{1} animals has been previously reported[86]. One way to confirm whether these lines are null alleles would be to perform a western blot on lysate from each fly line, but I did not have a *slo* antibody readily available to perform this experiment. Alternatively, *in situ* hybridization could be performed to probe for *slo* transcripts.

Even though transcript is detected in the slo^{1} mutant, the mutation results in reduced potassium currents from muscle cells[87], suggesting it is a null allele, or at the very least a severe hypomorph that prevents ion conductance. If the phenotypic effect of knocking down *slo* just in astrocytes with $slo^{RNAi\text{-}104421}$ resulted from reduced potassium current, a severe hypomorph would still be predicted to result in

the same phenotypes. However, if the effect of knocking down *slo* with $slo^{RNAi\text{-}104421}$ on astrocytes did not mechanistically depend on reduced current, morphological effects would not be observed. Additional function of pore-forming subunits of ion channels have been previously described, such as the activation of Ca^{2+}/calmodulin-dependent protein kinase II (CaMKII) by the alpha subunit of the voltage-gated potassium channel ether-à-go-go (eag)[88]. Since slo^{1} had morphologically normal astrocyte cell bodies, this suggests that *slo* conductance was not required for the observed phenotypes from $slo^{RNAi\text{-}104421}$. *slo* has 23 splice variants and it is possible that different neuronal and glial cell types express different isoforms. Since the exact mutation of the slo^{1} mutant has not been identified, it is possible that this mutation only manifests in isoforms expressed by neurons/muscle and not in astrocytes, leading to a normal astrocyte morphology. One way to distinguish these possibilities is creating a new mutant line that definitively deletes all isoforms of *slo*. I could then stain with GAT to examine the cell bodies of astrocytes to determine if an independently-generated mutant line recapitulated the phenotype.

Another possibility remains that the effects of knocking down *slo* with $slo^{RNAi\text{-}104421}$ is mediated by loss of *slo* interaction with additional signaling or scaffolding molecules. Some molecules shown to physically interact with *slo* in the fly are *slob*, a protein kinase, and *dysc*, a PDZ-family protein that regulates slo localization[84, 89]. In mammals, additional genes code for auxiliary beta-subunits that are differentially expressed by different cell types and tissues. The beta-subunits can alter properties of the alpha-subunit, such as gating kinetics, inactivation, and susceptibility to pharmacological blockers[70]. One way to test this possibility is to express RNAi lines targeted at the genes for the beta-subunits or other interactors with *slo* and observe whether an abnormal cell body phenotype or behavioral defects occur. If they do, it is likely that loss of interactions between *slo* and other signaling molecules results in these phenotypes.

If $slo^{RNAi\text{-}104421}$ results in phenotypes by knocking down another gene that is not *slo*, it would be difficult to determine exactly which gene is responsible. One way would be to express the RNAi in one

cell type and perform RNA sequencing and compare to a control without RNAi expression to look for differential gene expression. However, if the efficiency of *slo*$^{RNAi\text{-}104421}$ to hit its target is low, it may not produce an appreciable change in gene expression that can be measured with RNA sequencing. This method would also require harvesting a relatively large amount of homogenous tissue because of the cell-specific nature of using RNAi, which may not be feasible when trying to analyze fly astrocyte-specific gene expression.

All of this still leaves the question of how knocking down one gene in just astrocytes is affecting the entire nervous system enough to result in such dramatic motor dysfunction. One possibility is that all of the astrocytes are "sick" and are simply not functioning properly, which could be supported by the small cell body phenotype. However, the infiltration of astrocyte processes into the neuropil is grossly normal, indicating that the astrocytes are healthy enough to grow and develop normally to that point.

More experiments would be required to continue characterization of the phenotypes associated with astrocyte-specific expression of this RNAi line. Experiments investigating the number of synapses, and whether they are structurally normal, could give insight into how astrocytes may be causing the behavioral phenotypes. Increased formation of excitatory synapses or decreased formation of inhibitory synapses could lead to the behavioral phenotypes observed and would be consistent with the known role of astrocytes in promoting synapse formation. If the number of synapses was found to be normal, the phenotypes could also arise from problems with the astrocyte's ability to buffer ions—my initial hypothesis. Increases in the extracellular concentration of potassium ions can lead to hyperexcitability of neurons and a disruption of excitation/inhibition balance. Either of these possibilities would explain how expression of *slo*$^{RNAi\text{-}104421}$ in astrocytes worsens the seizure phenotype induced by the bang-sensitive mutation *eas.* Ultimately though, without the identification of the gene targeted by this RNAi line, a specific mechanism remains elusive and further experiments will not be conducted.

Ultimately, the phenotypes caused by astrocyte-specific expression of *slo*$^{RNAi\text{-}104421}$ could not be conclusively mapped to *slo*. However, the data presented above add to the growing body of evidence that astrocytes are required for the nervous system to function normally and that disrupting astrocytes can profoundly modify neural circuit outputs and alter behavior.

Materials and Methods

Drosophila strains

slo$^{RNAi-104421}$ (VDRC, v104421)

slo$^{RNAi-55405}$ (RRID:BDSC_55405)

slo$^{RNAi-6723}$ (VDRC, v6723)

slo$^{RNAi-26247}$ (RRID:BDSC_26247)

GMR25H07-GAL4 (alrm-max) (RRID:BDSC_49145)

GMR83E12-GAL4 (ensheathing-glia driver) (RRID:BDSC_40363)

GMR54H04-GAL4 (cortex glia driver) (RRID:BDSC_39090)

UAS-mCD8-GFP (RRID:BDSC_5137)

slo^{1} (RRID:BDSC_4587)

slo^{11481} (RRID:BDSC_29918)

w1118 (RRID:BDSC_3605)

alrm >nls-LexA>Gal4 13xLexAop-mCD8GFP, UAS-CD8-mCherry ftz-FLP (flp-out stock) (Generated by Tobi Stork, PhD)

Dissections

Wandering third instar larval brains were dissected in PTX (0.1% Tx-100, 1XPBS) and fixed in 4% formaldehyde in PTX on ice for no longer than 1 hour. The brains were then removed from ice and fixed for 20 minutes at room temperature. Brains were then washed 10 x 5 minutes with PTX. For imaging of endogenous fluorescence, brains were immediately mounted in Vectashield anti-fade reagent (Vector Laboratories) and imaged within the next week.

Immunohistochemistry

If staining occurred after dissection and fixation, larval brains were probed with appropriate primary antibodies for 1 night at 4°C. Samples were washed 10 x 5 minutes with PTX, probed with appropriate secondary antibodies for 1 night at 4°C, washed 10 x 5 minutes with PTX and then stored in Vectashield anti-fade reagent (Vector Laboratories).

Antibodies were used at the following dilutions: 1:4000 Rabbit Anti-GAT (lab-generated); 1:1000 Chicken Anti-GFP (AbCam); 1:250 Donkey Anti-Chicken (Jackson Immunoresearch); 1:250 Donkey Anti-Rabbit (Jackson Immunoresearch).

Confocal Imaging

Tissues were mounted in Vectashield anti-fade reagent and imaged using a Zeiss 880 confocal microscope. All images were taken using a PlanAprochromat 40X oil objective (NA=1.3) or a PlanAprochromat 63X oil objective (NA=1.4).

Quantification of Cell Bodies

Single z sections of astrocyte cell bodies were used for analysis using ImageJ. Individual cell bodies were traced with the polygon selection tool and designated a region of interest (ROI). For global RNAi and mutants, a minimum of 10 cell bodies were traced in each z section. For each genotype, 3-4 animals and a range of 47-68 cells were analyzed. For flp-out clones, a minimum of 4 cell bodies of each fluorescent label (mCherry or GFP) were traced in each z-section. For both genotypes, 3 animals and 32-42 cells were analyzed. Cell body area was quantified in square microns using the ImageJ 'Measure' tool for the subset of ROIs in each z section.

Adult Negative Geotaxis Assay

This assay was adapted from Ali et al[85]. Up to 10 flies of a given genotype were placed in a vial and sorted by sex. Flies were aged 1-3 days prior to testing and kept in a 25 C incubator. At the time of

testing, each group of flies were transferred to an empty polystyrene vial, which was taped to a second vial. The edges of the two vials were taped together to produce a smooth surface for the flies to walk along up the sides of the vial. A line was drawn around the circumference of the lower vial 8 cm from the bottom. After flies were transferred to the negative geotaxis apparatus, they were allowed to acclimate for 1 minute. Then, the flies were tapped to the bottom of the vial and allowed to crawl up the sides of the vial. After 10 seconds, the number of flies above the 8 cm line were recorded. This was repeated 10 times with a one-minute interval between each trial.

Larval Tracking Behavioral Assay

Larvae were placed on agar (0.8%) plates before being run in the assay. A maximum of six larvae were placed on a large 0.8% agar gel above a high-speed camera. The larvae were enclosed to prevent light disturbance. A video using Pylon Viewer software was filmed for one minute where the larvae were allowed to freely wander over the agar. After one minute, the larvae were immediately removed and disposed of to prevent them eating through the agar. The distance traveled by each larva was determined using FIMTrack software.

Bang-Sensitive Behavioral Assay

Flies were aged 3–4 days before testing. 6–10 flies were transferred to fresh food vials and vortexed for 10 s to provide mechanical stimulus and induce paralysis in bang-sensitive animals. The numbers of flies standing and resuming normal behavior were noted at 10 s intervals until all flies had recovered from paralysis. Mean recovery time was calculated as the average time taken by an individual fly to recover from paralysis

Reverse Transcription PCR

RNA from whole larvae was isolated using Qiagen RNeasy Mini kit. cDNA was synthesized using Applied Biosystems High-Capacity cDNA Reverse Transcription Kit. Primers for *slo* used were

5'GCCGATGATTGTCTCAAGGT3' for the forward primer and 5'GATACGAAGGACGGGGGTAT3' for the reverse.

Statistical Analysis

GraphPad Prism was used to perform all statistical analysis. Brown-Forsythe one-way ANOVAs with Dunnett's T3 multiple comparisons test were performed to compare astrocyte cell bodies in Fig. 1E, Fig. 3C, Fig, 3I, and Fig. 4D. Control *alrm-max-GAL4*, $slo^{RNAi\text{-}104421}$, and $slo^{RNAi\text{-}55405}$ animals were analyzed together because all of these samples were collected and processed together. Therefore, the control conditions presented in Fig. 1E and Fig. 3C represent the same data set. A distinct control *alrm-max-GAL4* dataset was collected and analyzed with $slo^{RNAi\text{-}6723}$, and $slo^{RNAi\text{-}26247}$ and is presented in Fig. 3I. A two-way ANOVA with Sidak's multiple comparisons test was used to analyze differences in astrocyte cell bodies in flp-out clones in Fig. 1J. An ordinary one-way ANOVA with Tukey's multiple comparisons test was used to analyze larval motility in Fig. 5A. A two-way ANOVA with Sidak's multiple comparisons test was used to analyze adult negative geotaxis in Fig. 5B. An unpaired t-test with Welch's correction was used to analyze recovery from seizure in Fig. S1.

Data distribution was assumed to be normal but this was not formally tested. No statistical methods were used to pre-determine sample sizes, but our sample sizes are similar to those reported in previous publications. Data collection and analysis were not performed blind due to the conditions of the experiments. Data were not collected and processed randomly. Animals were assigned to the various experimental groups based upon genotype.

Figure 1

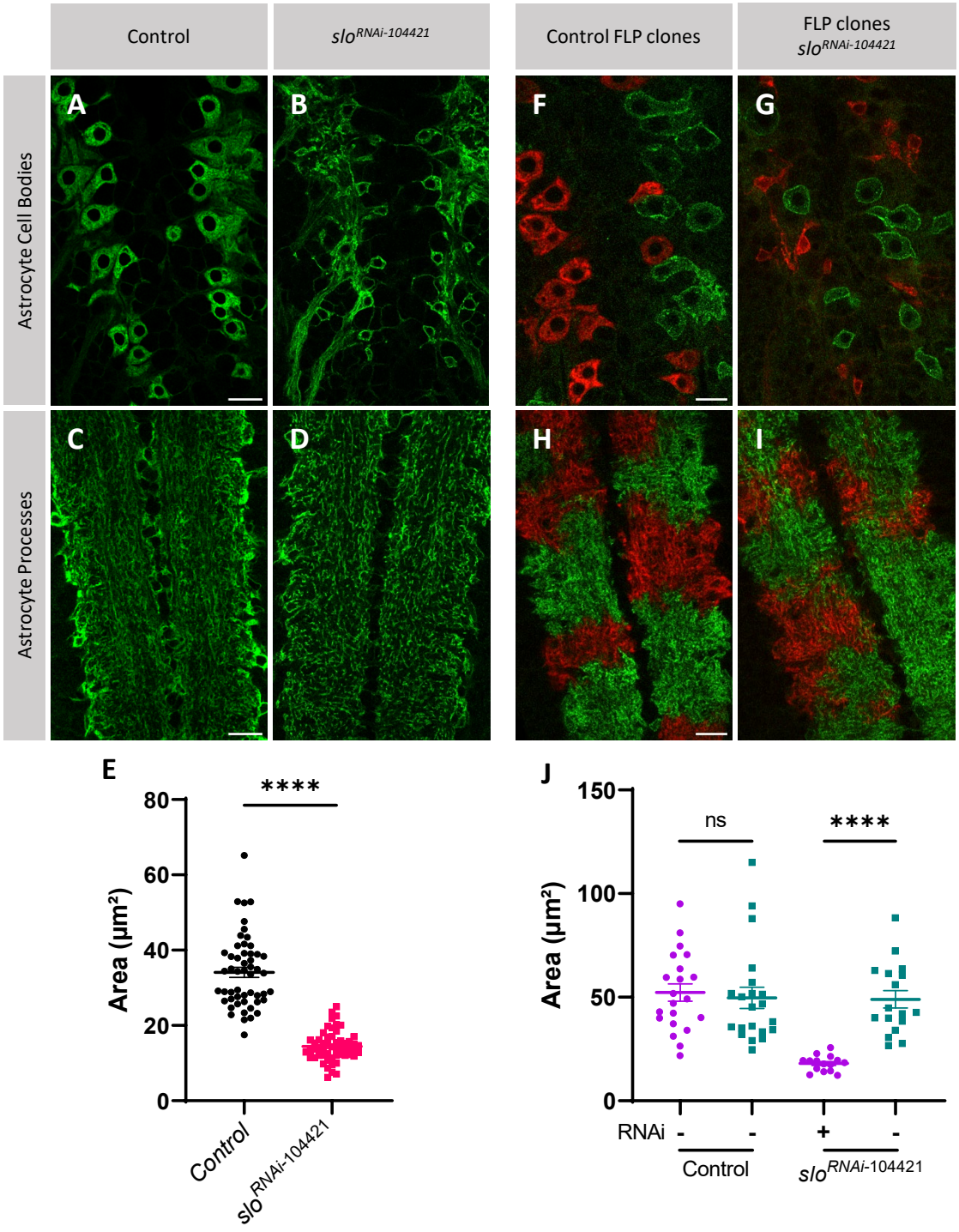
Control
slo RNAi-104421
Control FLP clones
FLP clones
slo RNAi-104421
Astrocyte Cell Bodies
Astrocyte Processes
A
B
C
D
F
G
H
I
E
Area (µm²)
80
60
40
20
0
****
Control
slo RNAi-104421
J
Area (µm²)
150
100
50
0
ns
****
RNAi
-
-
+
-
Control
slo RNAi-104421

Figure 1

Expression of *slo*$^{RNAi\text{-}104421}$ decreases astrocyte cell body size in global astrocyte RNAi knockdown and in flp-out clones, but process infiltration into the neuropil is unaffected

A-B) Single confocal plane of astrocyte cell bodies in L3 larval VNC: *alrm-max-GAL4 UAS-mCD8-GFP* expression was amplified with an α-GFP antibody to label astrocyte membranes in (A) control and (B) *slo*$^{RNAi\text{-}104421}$ with *alrm-max-GAL4*. *slo*$^{RNAi\text{-}104421}$ results in smaller, abnormal cell bodies compared to control. C-D) *UAS-mCD8-GFP* and α-GFP-labeled the fine processes of the astrocytes within the neuropil of the VNC in (A) control and (B) *slo*$^{RNAi\text{-}104421}$. Expression of *slo*$^{RNAi\text{-}104421}$ does not affect process infiltration. E) Quantification of cell body size in *alrm-max-GAL4 UAS-mCD8-GFP* animals shown in (A) and (B). At least 50 cells from 3-4 larvae were used for both genotypes. ****P < 0.0001. Mean and standard error bars shown. F-G) Small clusters of astrocyte clones were labeled using a flp-out system: *alrm >nls-LexA>Gal4 13xLexAop-mCD8-GFP*, *UAS-CD8-mCherry ftz-FLP* induces expression of either mCD8-GFP or CD8-mCherry. In control animals (F), both GFP (green) and mCherry (red) labeled astrocytes have similar cell body size. In animals expressing slo$^{RNAi\text{-}104421}$ concomitantly with mCherry (G), the cell bodies are smaller compared to control astrocytes within the same animal. H-I) Astrocyte process infiltration was comparable in control clones (G) and those expressing slo$^{RNAi\text{-}104421}$ (H). J) Quantification of cell body size in *alrm >nls-LexA>Gal4 13xLexAop-mCD8-GFP UAS-CD8-mCherry ftz-FLP* animals shown in (F) and (G). At least 15 cells with each fluorescent label from 3 animals were used in each genotype. ****P < 0.0001. Mean and standard error bars shown. (Scale bars: 10 µm)

Figure 2

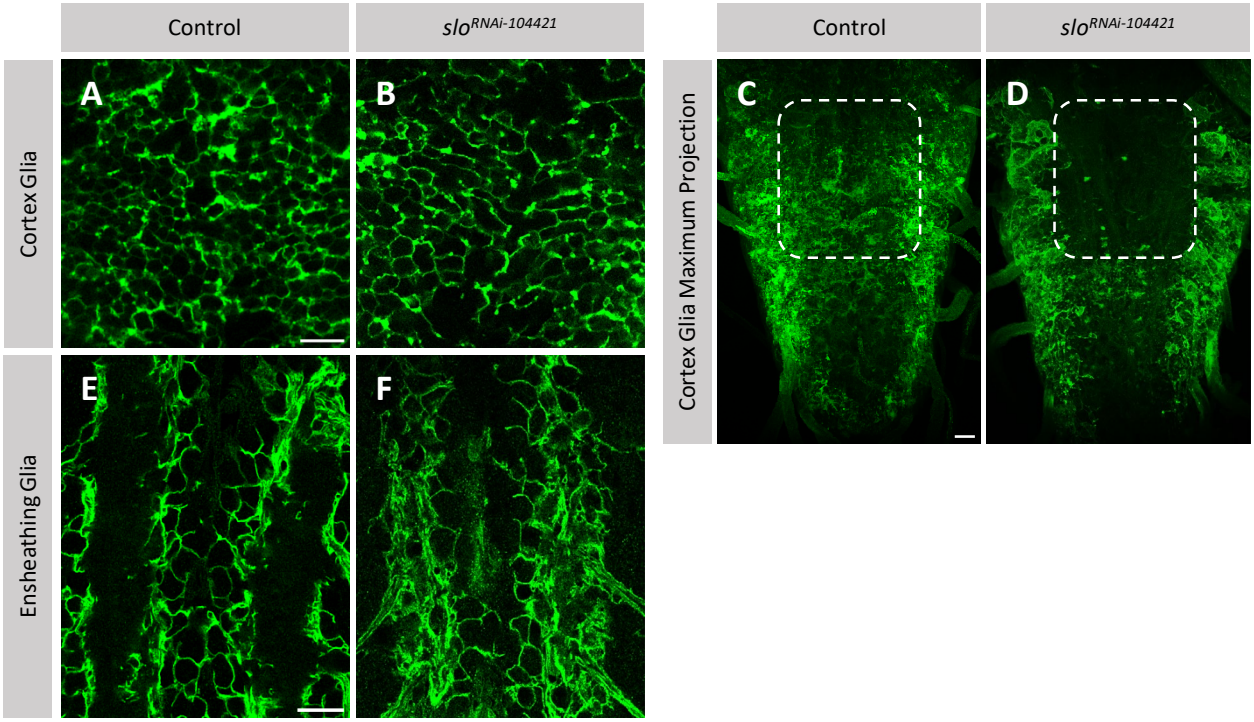

Figure 2

Expression of *slo*$^{RNAi-104421}$ in additional glia sub-types does not affect cell body size

A-B) Single confocal plane in L3 larval VNC: *GMR54H02-GAL4 UAS-mCD8-GFP* expression was amplified with an α-GFP antibody to label cortex glia cell membranes. Morphology of the cells was similar in both control (A) and *slo*$^{RNAi-104421}$ animals (B). C-D) Maximum intensity projection of L3 larval VNCs. Expression of *slo*$^{RNAi-104421}$ (D) leads to loss of cortex glia in the thoracic region of the VNC (dotted line inset) compared to control (C). E-F) Single confocal plane in L3 larval VNC: *GMR83E12-GAL4 UAS-mCD8-GFP* expression was amplified with an α-GFP antibody to label ensheathing glia cell membranes. Expression of *slo*$^{RNAi-104421}$ (F) has no effect on morphology compared to control (E). (Scale bars: 10 µm)

Figure 3

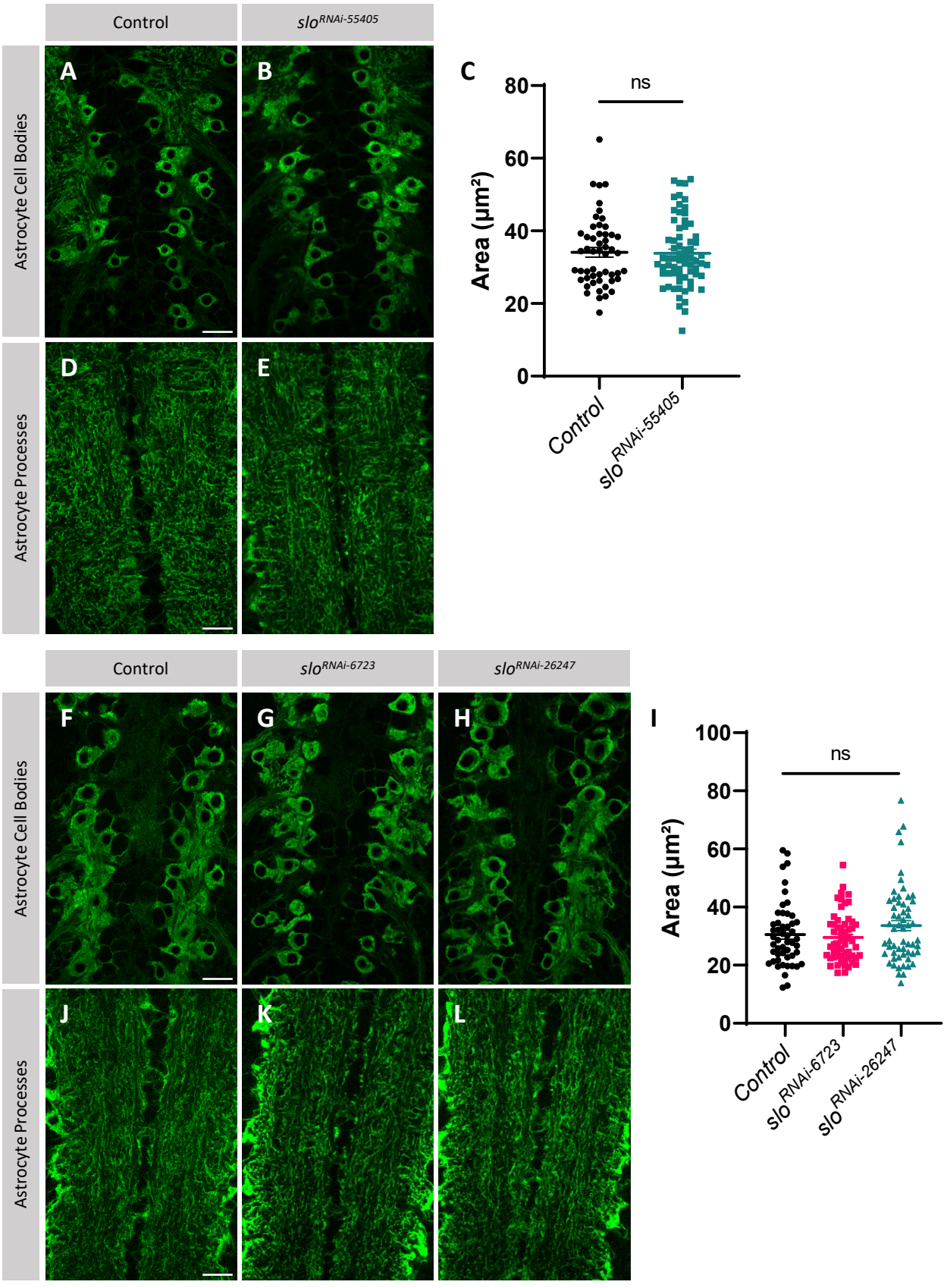
Control
slo RNAi-55405
Astrocyte Cell Bodies
Astrocyte Processes
A
B
C
D
E
ns
Area (µm²)
80
60
40
20
0
Control
slo RNAi-55405
Control
slo RNAi-6723
slo RNAi-26247
F
G
H
I
J
K
L
ns
Area (µm²)
100
80
60
40
20
0
Control
slo RNAi-6723
slo RNAi-26247

Figure 3

Additional *slo* RNAi lines expressed in astrocytes do not decrease cell body size

A-B) Single confocal plane of astrocyte cell bodies. *alrm-max-GAL4>UAS-mCD8-GFP* expression was amplified with an α-GFP antibody to label astrocyte membranes in control (A) and of $slo^{RNAi\text{-}55405}$ (B). Expression of $slo^{RNAi\text{-}55405}$ had no effect on astrocyte cell body size. C) Quantification of astrocyte cell body size in genotypes shown in (A) and (B). At least 50 cells from 3-4 animals were used for each genotype. Mean and standard error bars shown. D-E) Astrocyte processes were labeled with mCD8-GFP and an α-GFP antibody in control (D) and $slo^{RNAi\text{-}55405}$ (E). Expression of $slo^{RNAi\text{-}55405}$ had no effect on infiltration into the VNC. F-H) Single confocal plane of astrocyte cell bodies in control (F), $slo^{RNAi\text{-}26247}$ (G), and $slo^{RNAi\text{-}6723}$ (H). Expression of additional RNAi lines had no effect on astrocyte cell body size. I) Quantification of astrocyte cell body size. At least 50 cells from 3-4 animals were used in each genotype. Mean and standard error bars shown. J-L) Astrocyte processes were labeled with mCD8-GFP and an α-GFP antibody. No difference in process infiltration across any genotypes was observed. (Scale bars: 10 μm)

Figure 4

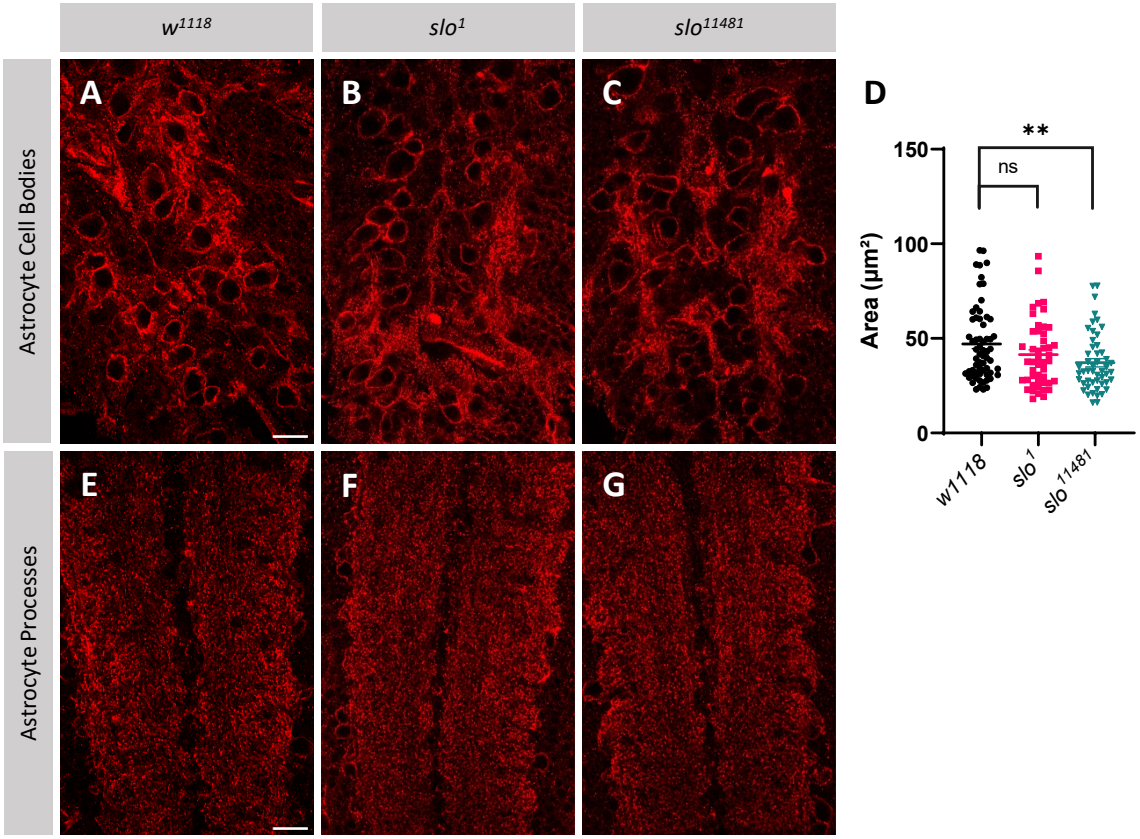

Figure 4

***slo* mutant alleles do not exhibit reduced astrocyte cell body size**

A-C) Confocal analysis of L3 larval VNCs. Single confocal plane of astrocyte cell body membranes labeled with α-GAT (a marker for astrocyte membranes) in control (A), *slo*^{1} (B), and *slo*^{11481} (C). *slo*^{1} has normal cell body size compared to controls whereas *slo*^{11481} animals have slightly smaller cell bodies than controls. D) Quantification of astrocyte cell body size. At least 47 cells from 3-4 larvae were used for all genotypes. Mean and standard error bars shown. E-G) Process infiltration (Scale bars: 10 µm)

Figure 5

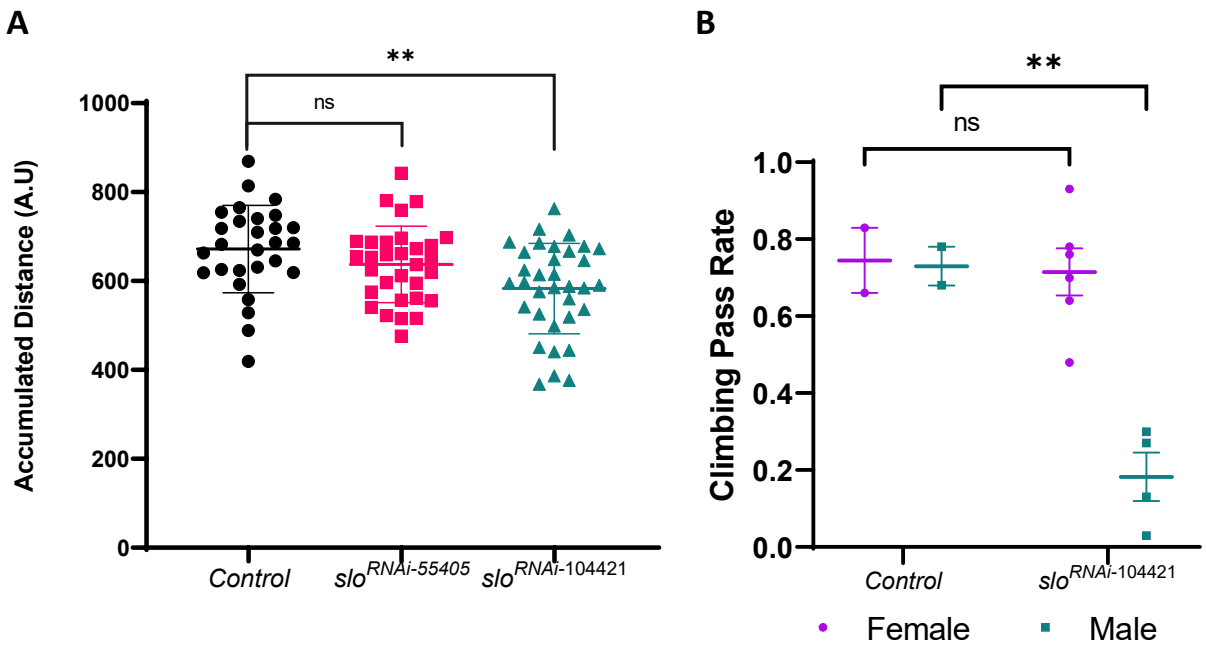

Figure 5

Astrocyte-expression of *slo*$^{RNAi-104421}$ results in larval and adult motor defects

A) Larval locomotion was measured by the distance traveled in one minute. *alrm-max-GAL4 slo*$^{RNAi-104421}$ traveled significantly shorter distances than *alrm-max-GAL4* driver alone. **P=0.0013, at least 28 larvae were used for each genotype. Mean and standard error bars shown. B) Negative geotaxis assay analysis of adult motor behavior demonstrates *alrm-max-GAL4 slo*$^{RNAi-104421}$ males are significantly impaired compared to *alrm-max-GAL4* controls. **P=0.005. Females in the RNAi condition were unaffected. Animals were tested in groups between five to ten animals. At least 10 animals were used each genotype. Mean and standard error bars shown.

Figure S1

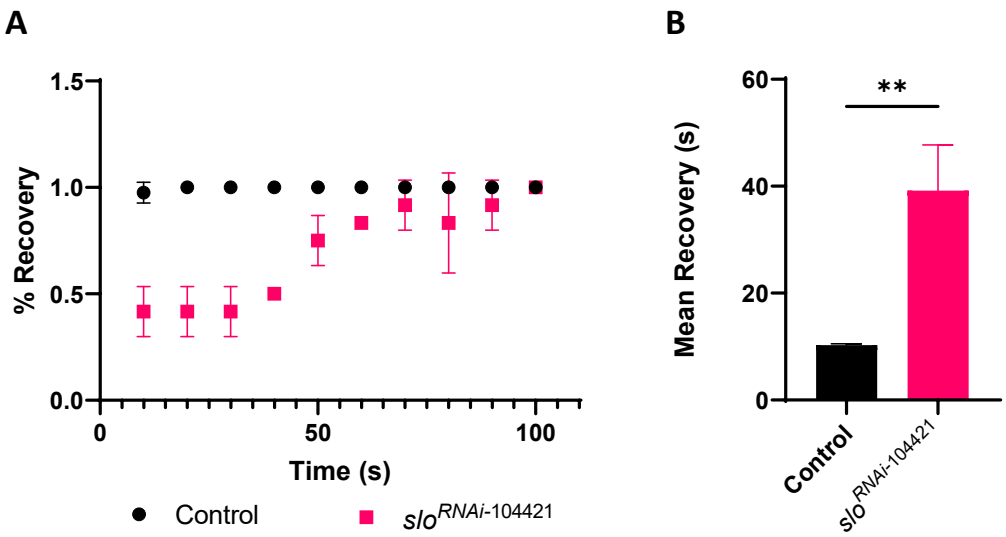

Supplemental Figure 1

Astrocyte-expression of *sloRNAi-104421* increases the time to recover from seizure behavior

A) Recovery curve of seizure behavior of *eas*^{PC80} *alrm-max-GAL4* control flies compared to *alrm-max-GAL4 sloRNAi-104421*. Mean and standard error bars shown. B) *eas*^{PC80} *alrm-max-GAL4* control flies recover from seizure behavior within 10 seconds on average. *alrm-max-GAL4 sloRNAi-104421* flies recover on average after 40 seconds, significantly longer than controls. Flies were tested in groups of 6-10 and at least 10 flies were used for both genotypes. **P=0.0062. Mean and standard error bars shown.

Figure S2

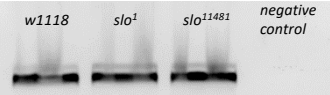

Supplemental Figure 2

RT-PCR on presumed *slo* mutants

(A) Reverse-transcription PCR on whole-larvae. Transcript was detected from *w1118, slo*^{1}, and *slo*^{11481} (lanes 1-3), but not from a negative control with no cDNA added (lane 4).

Appendix

Prior to the work described above, I contributed work to a lab mate Jimmy Hsu's project and paper that is currently under review. I summarize my contribution below.

Introduction

Injuries to the nervous system can result in changes to neuronal firing properties, death of neurons, and culminate in dysfunction of neuronal circuits. Injury to a neuron's axon activates a process called Wallerian degeneration (WD) where the portion of the axon distal to the site of injury undergoes explosive degeneration after a defined latent phase of several hours[90]. Later, the debris remaining is engulfed by surrounding glial cells[91]. *Drosophila melanogaster* is an excellent model organism with which to study injury signaling. Using screens in the fly, our lab identified the first endogenous executor of WD, dSarm/Sarm1[92]. Knocking out *dSarm/Sarm1* in neurons results in a complete blockade of axon degeneration after injury. Our lab has continued to define the pathway that dSarm signals through to initiate axonal degeneration, but other *in vivo* roles for dSarm remain to be identified.

A major limitation in the field of WD has been the focus on axon degeneration as the primary readout for analyzing the consequences of axonal injury. Obvious degeneration is a late response that occur several hours after the injury, but changes in other signaling events, like phosphorylation of MAP kinase, have been reported to occur in axons within 30 min after axotomy *in vitro*[93, 94]. Hsu et al (in submission) developed new assays to investigate early molecular signaling events that occur after injury and began to explore how these signaling events regulate changes in axon biology in both injured axons and neighboring intact (*i.e.*, uninjured) neurons. The *Drosophila* wing was used to study how both injured and uninjured "bystander" neurons respond to axotomy. Partial axotomy in the wing nerve led to a suppression of axonal transport and suppression of sensory transduction in both injured and bystander neurons. This phenotype required dSarm, the voltage-gated calcium channel Cacophony, and

components of the MAP kinase signaling cascade cell-autonomously. After several hours, bystander neurons recovered and injured neurons underwent WD.

Previous work examining cellular changes after axon injury has shown that increases in axonal calcium occur in response to axotomy[95]. It is now clear that dramatic increases of calcium in axons is both necessary and sufficient to drive axon degeneration. Injury-induced calcium influxes are mediated to some extent by voltage-gated calcium channels in severed axons, but whether calcium increases occur in adjacent, uninjured neurons has not been investigated.

Results

I sought to determine whether initial calcium influx after injury could account for injury-mediated differences in axon transport between wild-type animals and *dSarm* or *cac* mutants and whether initial calcium influx differed between injured and uninjured neurons. I laser-ablated L1 wing nerves and live imaged GCaMP6s fluorescence in neuronal cell body clones immediately following ablation. There was no difference in the amplitude of GCaMP6s signal between injured and intact neurons within individual genotypes. There was also no difference in the initial calcium responses following injury in mutants for *dsarm* or *axed* compared to controls. In *cacophony* null clones, there was a significant decrease in the maximum amplitude of the GCaMP signal of injured neurons compared to controls. It also took both intact and injured *cacophony* null neurons significantly longer to reach maximum amplitude, though it is worth noting a robust calcium response still occurred. This indicates Cacophony may partially contribute to initial calcium influxes after injury of the wing nerve. However, initial calcium bursts following injury are not sufficient to explain subsequent effects on axon transport in *dsarm* and *cacophony* null neurons.

Methods

Flies (3 to 7 days old) were anesthetized with CO2 and had the dorsal side of both wings and abdomen glued to a coverslip using a UV light-cured adhesive. Neurons were sparsely labeled and expressed GCaMP6s using a MARCM approach. Wing nerve ablation time-lapse images were taken on a 3I spinning disc confocal microscope with a Micropoint laser ablation system (430nm). An ablation region was selected by manually drawing a line across the wing nerve at the location for ablation to occur. All cell bodies analyzed were within 200 μm from the site of ablation. Time-lapse confocal images were analyzed using Fiji (ImageJ). Cell body average fluorescence intensity was analyzed by manually drawing regions of interest and F_0 was defined as the average fluorescence intensity for the ten seconds before ablation. Outliers for values of either max amplitude or the time to maximum amplitude were identified (ROUT method, Q=1%).

Figure S5:

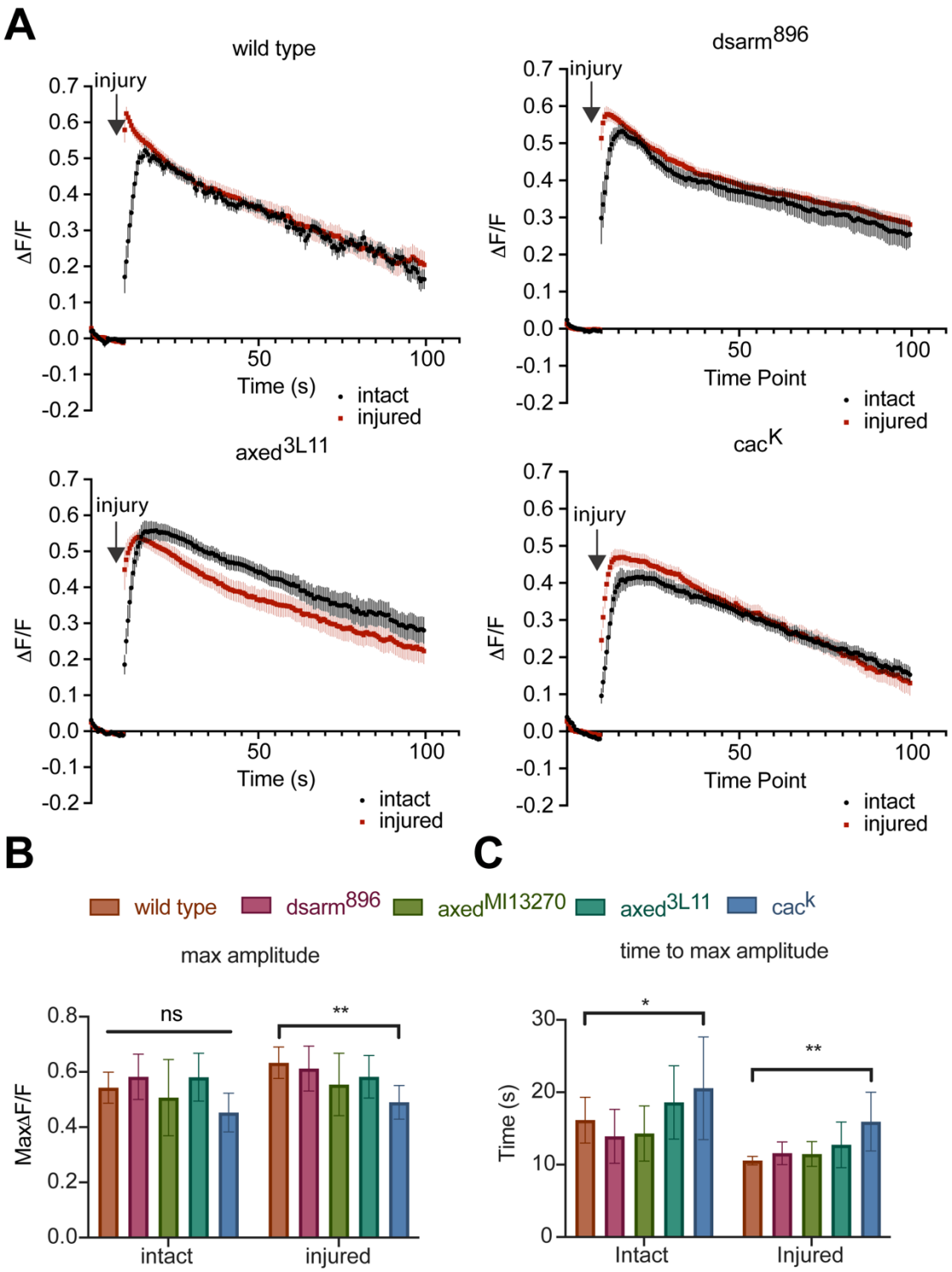
A
wild type
injury
ΔF/F
Time (s)
intact
injured
dsarm896
Time Point
axed3L11
cacK
B
wild type
dsarm896
axedMI13270
axed3L11
cack
max amplitude
MaxΔF/F
ns
**
intact
injured
C
time to max amplitude
Time (s)
*
**
Intact
Injured

Figure S5: Increase of calcium influx in the severed and intact axons after axotomy is mildly reduced in *cacophony* mutants. (Related to Figure 3)

(A) The GCamp6s intensity in different genotypes over time after injury is plotted. (Error bar = SEM, n = 9-15 wings)
(B, C) Maximum amplitude (B) and time to max amplitude (C) of GCamp6s intensity after injury in different genotypes. Two-way ANOVA with Sidak multiple comparisons test. (ns = not significant, *$p < 0.05$, **$p < 0.01$, n = 9-15 wings. Error bar = SEM.)

References

1. Jakel, S. and L. Dimou, *Glial Cells and Their Function in the Adult Brain: A Journey through the History of Their Ablation.* Front Cell Neurosci, 2017. **11**: p. 24.
2. Salter, M.W. and B. Stevens, *Microglia emerge as central players in brain disease.* Nat Med, 2017. **23**(9): p. 1018-1027.
3. Molofsky, A.V., et al., *Astrocytes and disease: a neurodevelopmental perspective.* Genes Dev, 2012. **26**(9): p. 891-907.
4. Beattie, R. and S. Hippenmeyer, *Mechanisms of radial glia progenitor cell lineage progression.* FEBS Lett, 2017. **591**(24): p. 3993-4008.
5. Tabata, H., *Diverse subtypes of astrocytes and their development during corticogenesis.* Front Neurosci, 2015. **9**: p. 114.
6. Bushong, E.A., et al., *Protoplasmic astrocytes in CA1 stratum radiatum occupy separate anatomical domains.* J Neurosci, 2002. **22**(1): p. 183-92.
7. Oberheim, N.A., et al., *Loss of astrocytic domain organization in the epileptic brain.* J Neurosci, 2008. **28**(13): p. 3264-76.
8. Araque, A., et al., *Tripartite synapses: glia, the unacknowledged partner.* Trends Neurosci, 1999. **22**(5): p. 208-15.
9. Ullian, E.M., et al., *Control of synapse number by glia.* Science, 2001. **291**(5504): p. 657-61.
10. Pfrieger, F.W. and B.A. Barres, *Synaptic efficacy enhanced by glial cells in vitro.* Science, 1997. **277**(5332): p. 1684-7.
11. Bosworth, A.P. and N.J. Allen, *The diverse actions of astrocytes during synaptic development.* Curr Opin Neurobiol, 2017. **47**: p. 38-43.
12. Mauch, D.H., et al., *CNS synaptogenesis promoted by glia-derived cholesterol.* Science, 2001. **294**(5545): p. 1354-7.
13. Goritz, C., D.H. Mauch, and F.W. Pfrieger, *Multiple mechanisms mediate cholesterol-induced synaptogenesis in a CNS neuron.* Mol Cell Neurosci, 2005. **29**(2): p. 190-201.
14. Ferris, H.A., et al., *Loss of astrocyte cholesterol synthesis disrupts neuronal function and alters whole-body metabolism.* Proc Natl Acad Sci U S A, 2017. **114**(5): p. 1189-1194.
15. Eroglu, C., et al., *Gabapentin receptor alpha2delta-1 is a neuronal thrombospondin receptor responsible for excitatory CNS synaptogenesis.* Cell, 2009. **139**(2): p. 380-92.
16. Xu, J., N. Xiao, and J. Xia, *Thrombospondin 1 accelerates synaptogenesis in hippocampal neurons through neuroligin 1.* Nat Neurosci, 2010. **13**(1): p. 22-4.
17. DeFreitas, M.F., et al., *Identification of integrin alpha 3 beta 1 as a neuronal thrombospondin receptor mediating neurite outgrowth.* Neuron, 1995. **15**(2): p. 333-43.
18. Singh, S.K., et al., *Astrocytes Assemble Thalamocortical Synapses by Bridging NRX1alpha and NL1 via Hevin.* Cell, 2016. **164**(1-2): p. 183-196.

19. Jones, E.V., et al., *Astrocytes control glutamate receptor levels at developing synapses through SPARC-beta-integrin interactions.* J Neurosci, 2011. **31**(11): p. 4154-65.

20. Christopherson, K.S., et al., *Thrombospondins are astrocyte-secreted proteins that promote CNS synaptogenesis.* Cell, 2005. **120**(3): p. 421-33.

21. Kucukdereli, H., et al., *Control of excitatory CNS synaptogenesis by astrocyte-secreted proteins Hevin and SPARC.* Proc Natl Acad Sci U S A, 2011. **108**(32): p. E440-9.

22. Allen, N.J., et al., *Astrocyte glypicans 4 and 6 promote formation of excitatory synapses via GluA1 AMPA receptors.* Nature, 2012. **486**(7403): p. 410-4.

23. Dunah, A.W., et al., *LAR receptor protein tyrosine phosphatases in the development and maintenance of excitatory synapses.* Nat Neurosci, 2005. **8**(4): p. 458-67.

24. Johnson, K.G., et al., *The HSPGs Syndecan and Dallylike bind the receptor phosphatase LAR and exert distinct effects on synaptic development.* Neuron, 2006. **49**(4): p. 517-31.

25. Diniz, L.P., et al., *Astrocyte-induced synaptogenesis is mediated by transforming growth factor beta signaling through modulation of D-serine levels in cerebral cortex neurons.* J Biol Chem, 2012. **287**(49): p. 41432-45.

26. Hughes, E.G., S.B. Elmariah, and R.J. Balice-Gordon, *Astrocyte secreted proteins selectively increase hippocampal GABAergic axon length, branching, and synaptogenesis.* Mol Cell Neurosci, 2010. **43**(1): p. 136-45.

27. Neniskyte, U. and C.T. Gross, *Errant gardeners: glial-cell-dependent synaptic pruning and neurodevelopmental disorders.* Nat Rev Neurosci, 2017. **18**(11): p. 658-670.

28. Penn, A.A., et al., *Competition in retinogeniculate patterning driven by spontaneous activity.* Science, 1998. **279**(5359): p. 2108-12.

29. Chung, W.S., et al., *Astrocytes mediate synapse elimination through MEGF10 and MERTK pathways.* Nature, 2013. **504**(7480): p. 394-400.

30. Stevens, B., et al., *The classical complement cascade mediates CNS synapse elimination.* Cell, 2007. **131**(6): p. 1164-78.

31. Awasaki, T., et al., *Essential role of the apoptotic cell engulfment genes draper and ced-6 in programmed axon pruning during Drosophila metamorphosis.* Neuron, 2006. **50**(6): p. 855-67.

32. Zhou, Z., E. Hartwieg, and H.R. Horvitz, *CED-1 is a transmembrane receptor that mediates cell corpse engulfment in C. elegans.* Cell, 2001. **104**(1): p. 43-56.

33. Tasdemir-Yilmaz, O.E. and M.R. Freeman, *Astrocytes engage unique molecular programs to engulf pruned neuronal debris from distinct subsets of neurons.* Genes Dev, 2014. **28**(1): p. 20-33.

34. Yang, J., et al., *Astrocytes contribute to synapse elimination via type 2 inositol 1,4,5-trisphosphate receptor-dependent release of ATP.* Elife, 2016. **5**: p. e15043.

35. Bialas, A.R. and B. Stevens, *TGF-beta signaling regulates neuronal C1q expression and developmental synaptic refinement.* Nat Neurosci, 2013. **16**(12): p. 1773-82.

36. Vainchtein, I.D., et al., *Astrocyte-derived interleukin-33 promotes microglial synapse engulfment and neural circuit development.* Science, 2018. **359**(6381): p. 1269-1273.

37. Risher, W.C., et al., *Astrocytes refine cortical connectivity at dendritic spines.* Elife, 2014. **3**.

38. Murphy-Royal, C., et al., *Astroglial glutamate transporters in the brain: Regulating neurotransmitter homeostasis and synaptic transmission.* J Neurosci Res, 2017. **95**(11): p. 2140-2151.

39. Conti, F., A. Minelli, and M. Melone, *GABA transporters in the mammalian cerebral cortex: localization, development and pathological implications.* Brain Res Brain Res Rev, 2004. **45**(3): p. 196-212.

40. Zafra, F., et al., *Glycine transporters are differentially expressed among CNS cells.* J Neurosci, 1995. **15**(5 Pt 2): p. 3952-69.

41. Tanaka, K., et al., *Epilepsy and exacerbation of brain injury in mice lacking the glutamate transporter GLT-1.* Science, 1997. **276**(5319): p. 1699-702.

42. Petr, G.T., et al., *Conditional deletion of the glutamate transporter GLT-1 reveals that astrocytic GLT-1 protects against fatal epilepsy while neuronal GLT-1 contributes significantly to glutamate uptake into synaptosomes.* J Neurosci, 2015. **35**(13): p. 5187-201.

43. Watanabe, T., et al., *Amygdala-kindled and pentylenetetrazole-induced seizures in glutamate transporter GLAST-deficient mice.* Brain Res, 1999. **845**(1): p. 92-6.

44. Watase, K., et al., *Motor discoordination and increased susceptibility to cerebellar injury in GLAST mutant mice.* Eur J Neurosci, 1998. **10**(3): p. 976-88.

45. Peghini, P., J. Janzen, and W. Stoffel, *Glutamate transporter EAAC-1-deficient mice develop dicarboxylic aminoaciduria and behavioral abnormalities but no neurodegeneration.* EMBO J, 1997. **16**(13): p. 3822-32.

46. Barbour, B., et al., *Prolonged presence of glutamate during excitatory synaptic transmission to cerebellar Purkinje cells.* Neuron, 1994. **12**(6): p. 1331-43.

47. Takahashi, M., M. Sarantis, and D. Attwell, *Postsynaptic glutamate uptake in rat cerebellar Purkinje cells.* J Physiol, 1996. **497 (Pt 2)**: p. 523-30.

48. Mennerick, S. and C.F. Zorumski, *Glial contributions to excitatory neurotransmission in cultured hippocampal cells.* Nature, 1994. **368**(6466): p. 59-62.

49. Ventura, R. and K.M. Harris, *Three-dimensional relationships between hippocampal synapses and astrocytes.* J Neurosci, 1999. **19**(16): p. 6897-906.

50. Henneberger, C., et al., *Long-term potentiation depends on release of D-serine from astrocytes.* Nature, 2010. **463**(7278): p. 232-6.

51. Panatier, A., et al., *Glia-derived D-serine controls NMDA receptor activity and synaptic memory.* Cell, 2006. **125**(4): p. 775-84.

52. Pascual, O., et al., *Astrocytic purinergic signaling coordinates synaptic networks.* Science, 2005. **310**(5745): p. 113-6.

53. Haydon, P.G. and M. Nedergaard, *How do astrocytes participate in neural plasticity?* Cold Spring Harb Perspect Biol, 2014. **7**(3): p. a020438.

54. Ma, Z., et al., *Neuromodulators signal through astrocytes to alter neural circuit activity and behaviour.* Nature, 2016. **539**(7629): p. 428-432.

55. Kofuji, P. and E.A. Newman, *Potassium buffering in the central nervous system.* Neuroscience, 2004. **129**(4): p. 1045-56.

56. Walz, W. and L. Hertz, *Intense furosemide-sensitive potassium accumulation in astrocytes in the presence of pathologically high extracellular potassium levels.* J Cereb Blood Flow Metab, 1984. **4**(2): p. 301-4.

57. Newman, E.A., *Regional specialization of retinal glial cell membrane.* Nature, 1984. **309**(5964): p. 155-7.

58. Newman, E.A., D.A. Frambach, and L.L. Odette, *Control of extracellular potassium levels by retinal glial cell K+ siphoning.* Science, 1984. **225**(4667): p. 1174-5.

59. Oakley, B., 2nd, et al., *Spatial buffering of extracellular potassium by Muller (glial) cells in the toad retina.* Exp Eye Res, 1992. **55**(4): p. 539-50.

60. Ma, B., et al., *Gap junction coupling confers isopotentiality on astrocyte syncytium.* Glia, 2016. **64**(2): p. 214-26.

61. Wallraff, A., et al., *The impact of astrocytic gap junctional coupling on potassium buffering in the hippocampus.* J Neurosci, 2006. **26**(20): p. 5438-47.

62. Ballanyi, K., P. Grafe, and G. ten Bruggencate, *Ion activities and potassium uptake mechanisms of glial cells in guinea-pig olfactory cortex slices.* J Physiol, 1987. **382**: p. 159-74.

63. Kivi, A., et al., *Effects of barium on stimulus-induced rises of [K+]o in human epileptic non-sclerotic and sclerotic hippocampal area CA1.* Eur J Neurosci, 2000. **12**(6): p. 2039-48.

64. Kucheryavykh, Y.V., et al., *Downregulation of Kir4.1 inward rectifying potassium channel subunits by RNAi impairs potassium transfer and glutamate uptake by cultured cortical astrocytes.* Glia, 2007. **55**(3): p. 274-81.

65. Djukic, B., et al., *Conditional knock-out of Kir4.1 leads to glial membrane depolarization, inhibition of potassium and glutamate uptake, and enhanced short-term synaptic potentiation.* J Neurosci, 2007. **27**(42): p. 11354-65.

66. Haj-Yasein, N.N., et al., *Evidence that compromised K+ spatial buffering contributes to the epileptogenic effect of mutations in the human Kir4.1 gene (KCNJ10).* Glia, 2011. **59**(11): p. 1635-42.

67. Nwaobi, S.E., et al., *The role of glial-specific Kir4.1 in normal and pathological states of the CNS.* Acta Neuropathol, 2016. **132**(1): p. 1-21.

68. Ransom, C.B., B.R. Ransom, and H. Sontheimer, *Activity-dependent extracellular K+ accumulation in rat optic nerve: the role of glial and axonal Na+ pumps.* J Physiol, 2000. **522 Pt 3**: p. 427-42.

69. Ransom, C.B., X. Liu, and H. Sontheimer, *BK channels in human glioma cells have enhanced calcium sensitivity.* Glia, 2002. **38**(4): p. 281-91.

70. Contet, C., et al., *BK Channels in the Central Nervous System.* Int Rev Neurobiol, 2016. **128**: p. 281-342.

71. Price, D.L., et al., *Distribution of rSlo Ca2+-activated K+ channels in rat astrocyte perivascular endfeet.* Brain Res, 2002. **956**(2): p. 183-93.

72. Kuschinsky, W., et al., *Perivascular potassium and pH as determinants of local pial arterial diameter in cats. A microapplication study.* Circ Res, 1972. **31**(2): p. 240-7.

73. Knot, H.J., P.A. Zimmermann, and M.T. Nelson, *Extracellular K(+)-induced hyperpolarizations and dilatations of rat coronary and cerebral arteries involve inward rectifier K(+) channels.* J Physiol, 1996. **492 (Pt 2)**: p. 419-30.

74. Filosa, J.A., et al., *Local potassium signaling couples neuronal activity to vasodilation in the brain.* Nat Neurosci, 2006. **9**(11): p. 1397-1403.

75. Girouard, H., et al., *Astrocytic endfoot Ca2+ and BK channels determine both arteriolar dilation and constriction.* Proc Natl Acad Sci U S A, 2010. **107**(8): p. 3811-6.

76. Wilcock, D.M., M.P. Vitek, and C.A. Colton, *Vascular amyloid alters astrocytic water and potassium channels in mouse models and humans with Alzheimer's disease.* Neuroscience, 2009. **159**(3): p. 1055-69.

77. Stork, T., et al., *Neuron-glia interactions through the Heartless FGF receptor signaling pathway mediate morphogenesis of Drosophila astrocytes.* Neuron, 2014. **83**(2): p. 388-403.

78. Ma, Z. and M.R. Freeman, *TrpML-mediated astrocyte microdomain Ca2+ transients regulate astrocyte-tracheal interactions in CNS.* bioRxiv, 2019: p. 865659.

79. Brand, A.H. and N. Perrimon, *Targeted gene expression as a means of altering cell fates and generating dominant phenotypes.* Development, 1993. **118**(2): p. 401-15.

80. Cho, S., et al., *Focal adhesion molecules regulate astrocyte morphology and glutamate transporters to suppress seizure-like behavior.* Proc Natl Acad Sci U S A, 2018. **115**(44): p. 11316-11321.

81. Doherty, J., et al., *Ensheathing glia function as phagocytes in the adult Drosophila brain.* J Neurosci, 2009. **29**(15): p. 4768-81.

82. Freeman, M.R., *Drosophila Central Nervous System Glia.* Cold Spring Harb Perspect Biol, 2015. **7**(11).

83. Homem, C.C. and J.A. Knoblich, *Drosophila neuroblasts: a model for stem cell biology.* Development, 2012. **139**(23): p. 4297-310.

84. Jepson, J.E., et al., *Regulation of synaptic development and function by the Drosophila PDZ protein Dyschronic.* Development, 2014. **141**(23): p. 4548-57.

85. Ali, Y.O., et al., *Assaying locomotor, learning, and memory deficits in Drosophila models of neurodegeneration.* J Vis Exp, 2011(49).

86. Scheckel, K. *Potassium channel expression in the larval Drosophila melanogaster CNS*. in *Annual Meeting of the American Association for the Advancement of Science*. 2011. Washington, DC.

87. Elkins, T., B. Ganetzky, and C.F. Wu, *A Drosophila mutation that eliminates a calcium-dependent potassium current.* Proc Natl Acad Sci U S A, 1986. **83**(21): p. 8415-9.

88. Kaczmarek, L.K., *Non-conducting functions of voltage-gated ion channels.* Nat Rev Neurosci, 2006. **7**(10): p. 761-71.

89. Jaramillo, A.M., et al., *Expression and function of variants of slob, slowpoke channel binding protein, in Drosophila.* J Neurophysiol, 2006. **95**(3): p. 1957-65.

90. Waller, A., *Experiments on the Section of the Glosso-Pharyngeal and Hypoglossal Nerves of the Frog, and Observations of the Alterations Produced Thereby in the Structure of Their Primitive Fibres.* Edinb Med Surg J, 1851. **76**(189): p. 369-376.

91. MacDonald, J.M., et al., *The Drosophila cell corpse engulfment receptor Draper mediates glial clearance of severed axons.* Neuron, 2006. **50**(6): p. 869-81.

92. Osterloh, J.M., et al., *dSarm/Sarm1 is required for activation of an injury-induced axon death pathway.* Science, 2012. **337**(6093): p. 481-4.

93. Yang, J., et al., *Pathological axonal death through a MAPK cascade that triggers a local energy deficit.* Cell, 2015. **160**(1-2): p. 161-76.

94. Walker, L.J., et al., *MAPK signaling promotes axonal degeneration by speeding the turnover of the axonal maintenance factor NMNAT2.* Elife, 2017. **6**.

95. Knoferle, J., et al., *Mechanisms of acute axonal degeneration in the optic nerve in vivo.* Proc Natl Acad Sci U S A, 2010. **107**(13): p. 6064-9.